AD-A080 927 NAVAL AIR DEVELOPMENT CENTER WARMINSTER PA AIRCRAFT --ETC F/G 11/4
COMPRESSION FATIGUE OF IMPACT DAMAGED GRAPHITE EPOXY SANDWICH B--ETC(U)
APR 78 L W GAUSE, S L HUANG

UNCLASSIFIED NADC-77305-60 NL

| OF |
AD
A080927

END
DATE FILMED
3 - 80
DDC

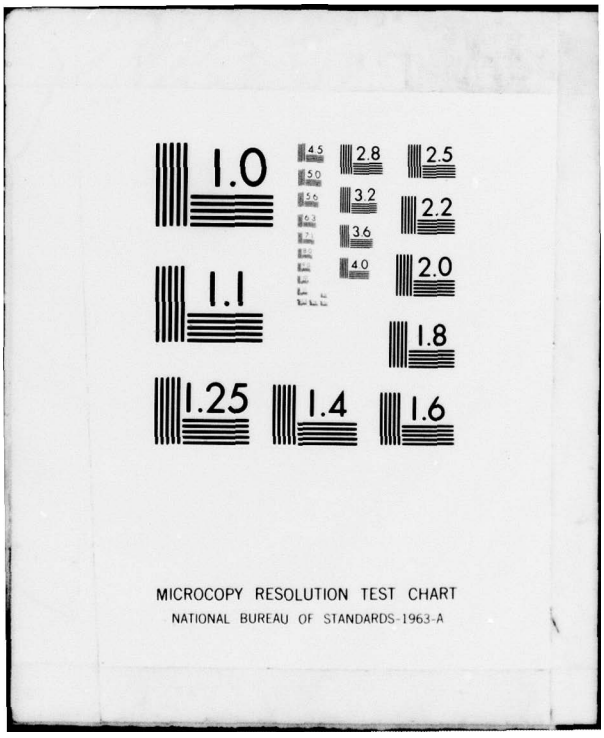
1.0
1.1
1.25
1.4
1.6
1.8
2.0
2.2
2.5
2.8
3.2
3.6
4.0
4.5
5.0
5.6
6.3
7.1
MICROCOPY RESOLUTION TEST CHART
NATIONAL BUREAU OF STANDARDS-1963-A

REPORT NO. NADC-77305-60

COMPRESSION FATIGUE OF IMPACT DAMAGED GRAPHITE EPOXY SANDWICH BEAMS

Lee W. Gause and Shih L. Huang
Aircraft and Crew Systems Technology Directorate
NAVAL AIR DEVELOPMENT CENTER
Warminster, Pennsylvania 18974

20 APRIL 1978

FINAL REPORT
AIRTASK NO. WR02303001
Work Unit DG 602

APPROVED FOR PUBLIC RELEASE; DISTRIBUTION UNLIMITED.

Prepared for
NAVAL AIR SYSTEMS COMMAND
Department of the Navy
Washington, D.C. 20361

NOTICES

REPORT NUMBERING SYSTEM - The numbering of technical project reports issued by the Naval Air Development Center is arranged for specific identification purposes. Each number consists of the Center acronym, the calendar year in which the number was assigned, the sequence number of the report within the specific calendar year, and the official 2-digit correspondence code of the Command Office or the Functional Directorate responsible for the report. For example: Report No. NADC-78015-20 indicates the fifteenth Center report for the year 1978, and prepared by the Systems Directorate. The numerical codes are as follows:

CODE	OFFICE OR DIRECTORATE
00	Commander, Naval Air Development Center
01	Technical Director, Naval Air Development Center
02	Comptroller
10	Directorate Command Projects
20	Systems Directorate
30	Sensors & Avionics Technology Directorate
40	Communication & Navigation Technology Directorate
50	Software Computer Directorate
60	Aircraft & Crew Systems Technology Directorate
70	Planning Assessment Resources
80	Engineering Support Group

PRODUCT ENDORSEMENT - The discussion or instructions concerning commercial products herein do not constitute an endorsement by the Government nor do they convey or imply the license or right to use such products.

APPROVED BY: E. J. Sturm DATE: 20 April 1978

E. J. STURM
Commander, USN
Deputy Director, ACSTD

UNCLASSIFIED

SECURITY CLASSIFICATION OF THIS PAGE (When Data Entered)

REPORT DOCUMENTATION PAGE

READ INSTRUCTIONS BEFORE COMPLETING FORM

1. REPORT NUMBER: NADC-77305-60
2. GOVT ACCESSION NO.:
3. RECIPIENT'S CATALOG NUMBER:

4. TITLE (and Subtitle): Compression Fatigue of Impact Damaged Graphite Epoxy Sandwich Beams.

5. TYPE OF REPORT & PERIOD COVERED: Final Report

6. PERFORMING ORG. REPORT NUMBER:

7. AUTHOR(s): Lee W. Gause, Shih L. Huang

8. CONTRACT OR GRANT NUMBER(s): WR02303

9. PERFORMING ORGANIZATION NAME AND ADDRESS:
Aircraft and Crew Systems Technology Directorate
Naval Air Development Center
Warminster, PA 18974

10. PROGRAM ELEMENT, PROJECT, TASK AREA & WORK UNIT NUMBERS: 61153N, R023-03, WR02303001 / W.U. DG 602

11. CONTROLLING OFFICE NAME AND ADDRESS:
Naval Air Systems Command (AIR-320B)
Department of the Navy
Washington, D.C. 20361

12. REPORT DATE: 20 Apr 1978

13. NUMBER OF PAGES: 50

14. MONITORING AGENCY NAME & ADDRESS (if different from Controlling Office): 53

15. SECURITY CLASS. (of this report): UNCLASSIFIED

15a. DECLASSIFICATION/DOWNGRADING SCHEDULE:

16. DISTRIBUTION STATEMENT (of this Report)

Approved for Public Release; Distribution Unlimited

17. DISTRIBUTION STATEMENT (of the abstract entered in Block 20, if different from Report)

18. SUPPLEMENTARY NOTES

19. KEY WORDS (Continue on reverse side if necessary and identify by block number)

Composite
Impact
Honeycomb Sandwich
Compression Fatigue

20. ABSTRACT (Continue on reverse side if necessary and identify by block number)

The resistance of composite aircraft structures to handling and impact loadings is an important consideration in assessing their suitability for long term operational service. The specific threat addressed in this study is that of low speed (0 to 30 m/s), hard object, transverse normal impact (dropped tool, runway stones, etc.). The objective is to characterize the damage which occurs to composite faced sandwich structures under realistic impact conditions and determine the effect of this damage on residual compression fatigue properties. The sandwich construction selected for study consisted of AS/3501-6

DD FORM 1 JAN 73 1473 EDITION OF 1 NOV 65 IS OBSOLETE S/N 0102-014-6601 |

UNCLASSIFIED

SECURITY CLASSIFICATION OF THIS PAGE (When Data Entered)

393532

(0/+α - 45/0) subs

graphite/epoxy face sheets of $[0/\pm45/0]_s$ construction bonded to HRP-3/16-5.5 honeycomb core. This construction is representative of sandwich construction generally used in flaps, spoilers, and access doors.

Static indentation tests were conducted on sandwich panels supported on a rigid foundation, and dropped weight impact tests were performed on simply supported sandwich beams. Comparison of the results of these tests indicates that static tests in conjunction with a simple 2-degree-of-freedom dynamic model can be used to accurately simulate low velocity, hard object impacts on sandwich structures for impact velocities up to 6.1 m/s. Test results of indentation versus static load is used in the dynamic model to predict the indentation which would occur for any particular impact case. The equivalent impact damage is then determined from the measured static indentation versus static damage. Damage type and extent were determined both visually and by ultrasonic pulse-echo inspection using Navy fleet maintenance equipment. Initial damage to the sandwich consists of slight core crushing under the contact point with no damage to the face sheet. Additional displacement of the indenter causes delaminations to occur in the face sheet with no visual indication of damage other than a slight depression at the contact point. Further indentation leads to face sheet bending failure with obvious visual damage.

Compression fatigue tests were conducted with a stress ratio $R = -\infty$. Results showed no difference in fatigue properties between drop weight impact damaged specimens and statically simulated impact damage specimens. Impact damage which cannot be visually detected can significantly degrade structural properties. For a maximum compressive fatigue strain of 0.0060, damage larger than 11.5 mm diameter will cause fatigue failure. Visually detectable damage, however, can be tolerated in low strain applications, i.e. maximum compressive strain less than .0033. No significant damage growth was observed during fatigue cycling, and where damage growth was noted, no correlation between damage growth and fatigue failure could be made. Fatigue failures of the damaged sandwich panels occur by compression buckling of the face sheet in the region of the impact crushing core and the delaminated face sheet.

TABLE OF CONTENTS

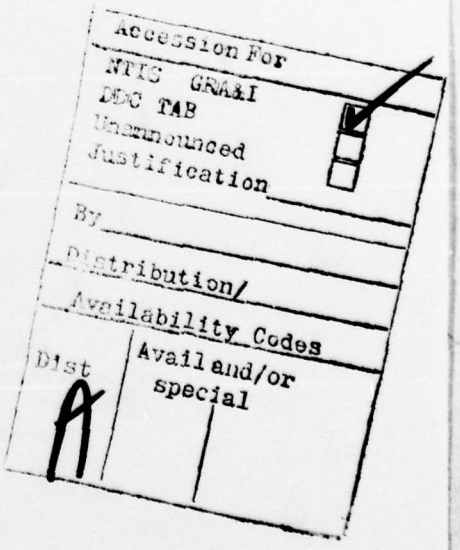

LIST OF TABLES

LIST OF FIGURES

LIST OF FIGURES

INTRODUCTION

An attractive application for advanced composite materials is as face sheets for honeycomb-stabilized sandwich structures due to the high structural efficiency intrinsic with this type construction. A source of concern in applying this configuration to aircraft is its resistance to low velocity impact loading which might be experienced in operational service, such as runway stones, dropped tools, and hail. Although previous research is limited, several papers are available on the impact tolerance and post impact residual properties of thin-skinned composite sandwich structures. References 1 and 2 conducted experimental investigations of the impacted surface for visual damage and the load-carrying capacity of graphite/epoxy and Kevlar/epoxy composite sandwich structures after low velocity impact. Damage was measured by visual observations only. Significant reductions in tensile and compression strengths were caused by sub-visual damage. Reference 3 carried out an elastic analysis of a sandwich panel indented by a rigid sphere to determine stresses and deformations, and to identify critical parameters. The analysis showed core crushing is possible at relatively low loads and that face sheet strains depend primarily on the indenter radius and the relative stiffnesses of core and face sheet. Impact tests were conducted on graphite/epoxy and S-glass/epoxy sandwich structures. Graphite/epoxy was determined to be highly susceptible to impact damage due to its low failure strain.

The results of these previous studies demonstrate graphite/epoxy sandwich construction to be susceptible to impact damage and to suffer static strength reductions when compared to unflawed reference panels. The objective of this study was to determine the sensitivity of graphite/epoxy sandwich construction to low velocity impact threats with the object of determining criteria for use in design and to develop a model to relate laboratory test results to design situations. The approach used to meet these objectives were: (1) examine damage mechanisms of graphite/epoxy face sheets subject to hard object impact type loading, (2) determine the damage propagation characteristics under compression fatigue, and (3) provide a method to predict the impact response of a sandwich structure based on a simple static test.

TEST SPECIMENS

The test specimens used in this investigation were rectangular sandwich beams 3 in. (76.2 mm) wide by 14 in. (355.6 mm) long. Face sheets were 8 ply AS/3501-6 graphite/epoxy laminates of $(0^{\circ}/\pm 45^{\circ}/0^{\circ})_{s}$ layup. Large panels were fabricated by hand layup and autoclave cure following the cure cycle suggested by the prepreg supplier. These laminates were then bonded to honeycomb core to form two large honeycomb panels from which the individual test specimens were machined. The adhesive used was FM-123-5 film adhesive. The core materials were 0.50 in (12.7 mm) thick and consisted of HRP-3/16-5.5 in the central 3 in. x 3 in. (76.2 mm x 76.2 mm) test section and AL-1/8-5052-.003-12 elsewhere, see Figure 1. These specimens, manufactured by General Dynamics, Convair Division, are of the same construction as the sandwich specimens studied in a concurrent program, reference 4. The test section of these specimens is intended to be representative of typical composite full depth honeycomb sandwich construction for a secondary structure.

STATIC INDENTATION TESTS

Static tests were conducted with a Baldwin machine using steel indenters with 0.25 in. (6.4 mm) and 1 in. (25.4 mm) tip radius. The sandwich test panels were fully supported on a rigid foundation, Figure 2. Load versus indentation was recorded during each test on an x-y recorder. Loading was continued until the indenter had penetrated the face sheet to various predetermined depths, the depth of indentation being used as a parameter to which any resulting damage will be related. Note that depth of indentation and depth of damage are not necessarily equal. From the load-indentation history, the elastic energy for indentation could be obtained as well as a simple spring constant to represent the contact force between indenter and sandwich panel. Following each test the surface of the sandwich panel was inspected for damage both visually and by NDE using ultrasonic pulse-echo techniques. The ultrasonic detector unit used was a portable AN/GSM-238 Ultrasonic Flaw Detector Set. This equipment is currently available in Navy fleet maintenance organizations, therefore, damage detected during this test program is representative of damage levels detectable in Navy field service.

STATIC TEST RESULTS

Results of tests performed by statically pressing the indenter into a sandwich panel fully supported on a rigid foundation, show there are several distinct segments to the load-indentation curve. Although similar for each indenter, the shape of this curve depends greatly on the radius of the indenter, see Figure 3. The initial portion of the load-indentation curve is linearly elastic. No damage is incurred by the specimen in this region. Upon additional load the core cripples, (the boundary is marked Damage Threshold in Figure 3), while the face sheet remains intact, Figures 4 and 5. Although visual inspection and NDE indicate no damage to the specimen at this point, it is obvious from the knee in the load-indentation curve that, while undectable by the above means, damage has occurred. Additional displacement of the indenter past the threshold point is again essentially linear in load-indentation until face sheet bending failure occurs and damage becomes readily visible. Between damage threshold and face sheet bending failure some face sheet delamination occurs and damage becomes easily detectable by NDE, Figures 6 and 7. At the visual threshold, damage can be seen as a slight depression in the face sheet, but it is not obvious and the observer must know the contact location to be able to detect the damage. Additional loading past face sheet bending failure results in another load-indentation curve slope change as both the face sheet and core break and crush under additional indenter displacement, Figures 8 and 9. The load will continue to increase until the face sheet has been damaged sufficiently to allow the indenter tip diameter to pass through, after which the load-indentation curve is horizontal (zero slope) because the displacement is resisted predominately by core crushing. Note that for the 1/4 inch (6.4 mm) radius indenter this occurs just after face sheet bending failure. Results of all static tests are presented in Table I. Figure 10 presents the idealized load versus indentation results for the static tests. Figure 11 is a plot of the damage area determined by NDE versus indentation. Damage area was calculated considering the damage to be elliptical in shape.

$$\text{Damage Area} = \frac{\pi}{4} AB$$

where,

A = maximum length of damage region

B = maximum width of damage region

Although the data has considerable scatter, a definite correlation between indentation and damage area is apparent.

D Y N A M I C M O D E L

Reference 3 observes that static tests give a good representation of the impact response of sandwich panels at low impact speeds representative of drop tests. Assuming the static and dynamic behavior to be identical, it is possible to model the dynamic impact of a hard object on a sandwich structure as a two-degree-of-freedom (2-DOF) spring mass problem, Figure 12. In this figure

m_1 = effective mass of sandwich structure

k_1 = effective structural stiffness

m_2 = impact mass

k_2 = contact stiffness

w_1 = coordinate of structure

w_2 = coordinate of impact mass

and the contact force is approximated by

$$F = k_2 (w_2 - w_1), \text{ where } k_2 = 0 \text{ if } w_2 < w_1$$

The equations of motion of this system are:

$$m_1\ddot{w}_1 + (k_1 + k_2) w_1 - k_2 w_2 = 0$$

$$m_2\ddot{w}_2 + k_2 (w_2 - w_1) = 0 \qquad \text{for } w_2 - w_1 \geq 0$$

while the sandwich and impactor are in contact.

During periods when the two are separated, the sandwich structure vibrates freely, so that

$$m_1\ddot{w}_1 + k_1 w_1 = 0$$

$$\ddot{w}_2 = 0 \qquad \text{for } w_2 - w_1 < 0$$

where this second condition corresponds to free flight of the impactor. Using the initial conditions

$$w_1 (0) = w_2 (0) = 0$$

$$\dot{w}_1 (0) = 0$$

$$\dot{w}_2 (0) = v \text{ (velocity at impact)}$$

Reference 5 developed a numerical solution for this 2-DOF spring mass problem while studying hard object impact on solid laminate beams. This solution was utilized with slight modification for the present case of impact on sandwich beams to develop an impact mass versus indentation curve. The modification was required to account for core crushing. A plastic-elastic load-indentation curve was assumed, Figure 13. A contact stiffness of k_2 was assumed during loading along the plastic portion of the curve and a contact stiffness of k_{2E} along the elastic portion. For the present study a value of $k_{2E} = 2k_2$ was used. The value of k_2 is approximated from the experimental load-indentation curve by a linear load-indentation relation assumed so that the area under the approximate curve (elastic energy for indentation) equals the area under the experimental curve at the expected indentation, Figure 14. An indentation versus impact mass curve for impacts of 20 ft/sec (6.1 m/s) was generated for impact on the sandwich beams used in this experiment, Figure 15. The beams were assumed simply supported on a span of 12 inches (304.8 mm) with k_1 = 4132 lbf/in (723.6 kN/m), m_1 = 0.135 lbm (61.2 g).

If static and dynamic behavior are the same, damage areas obtained from the static indentation tests should equal the damage areas resulting from impact tests for equivalent indentation depths.

I M P A C T T E S T S

Drop weight tests were performed employing variable weight steel indenters of 1/4 inch (6.4 mm) and 1 inch (25.4 mm) tip radii dropped from a height of 6.211 ft. (1.89 m) to give an impact velocity of 20 ft/sec (6.1 m/s). The sandwich specimens were simply supported as beams with a 12 in. (304.8 mm) span. Results are presented in Table II and Figures 16 through 23. Table II also includes the equivalent static indentation calculated using the 2-DOF dynamic model for each impact test.

Comparison between static penetration test results and dynamic impact test results for fixed indenter radius show essentially identical damage resulting from equivalent indentations. The predicted damage area for dynamic impact is obtained by using equivalent indentation from Figure 15 and NDE damage area for this indentation from Figure 11. This predicted damage area is plotted against the measured damage area and is presented in Figure 24 where good correlation is seen to exist up to a predicted damage area of 1.0 in.^{2} (6.45 cm^2) approximately, which corresponds to a penetration depth of 0.1 in (2.54 mm) approximately. Thus, the assumption of identical static and dynamic damage mechanisms for sandwich panels is viable, at least to describe impacts up to 20 ft/sec

(6.1 m/s) and for indentations less than 0.1 in. (2.54 mm). Therefore the potential damage to a sandwich structure resulting from a range of low speed, hard object impact threats can be determined from static tests using results from the simple 2-DOF dynamic model.

F A T I G U E T E S T S

A. MODIFIED FOUR-POINT BENDING FIXTURE

Compressive fatigue tests were performed on specimens damaged by static indentation and by drop weight impact, using a four-point bend test fixture with off-center load introduction at the top support, Figure 25. The specimens were oriented to place the damaged face sheet in compression. The damaged region of the face sheet was always on the center of the specimen. The off-center loading was used to impose a small shear stress through the specimen test section. The ratio of the average shear stress through the sandwich cross section to the inplane face sheet stress at the damaged region is 1:588. Test specimens were loaded cyclically by a hydraulic actuator to a stress ratio for the test face sheet of $R = -\infty$ at a frequency of 1.25 Hz until either failure or 60,000 cycles had been achieved. To facilitate testing, any specimen which sustained 60,000 cycles without failure was considered to be a run-out. Specimens were removed for visual and NDE examination at 2000, 4000, 10,000, 20,000, 40,000, and 60,000 cycles in order to observe and measure damage growth.

A undamaged specimen was tested for a reference.

B. FATIGUE TEST RESULTS

Fatigue tests were conducted to a maximum compressive stress at the center of the test face of 58.7 ksi (405 MPa). The strain corresponding to this stress is .0059. This reference stress level was determined by taking two-thirds of 90% of B-basis tensile strength for the face sheet laminate and is considered to be the design ultimate stress (and strain) for a fully bonded (no manufactured holes) structure. Due to the off-center loading, maximum shear stress in the core was 100 psi (689 kPa). Fatigue test results are summarized in Table III. The first entry in Table III, the results for the undamaged specimen, demonstrates the ability of the basic specimen to withstand fatigue cycling at the reference strain level. Initial tests were performed on the large-damage specimens (damage readily visible) to access the effect this level of damage would have on compressive fatigue life. All specimens failed during the first cycle (static failure). Failure stress (and strain) ranged from 65% to 100% of reference (Table III, specimens 1 through 6). The failures were all buckling failure of the compressive face through the center of the damage area, Figure 26.

The next series of fatigue tests were run on specimens with damage insufficient to be detected either visually or ultrasonically. This is the most critical test point because if this "undectable" damage affects the sandwich properties, it could severly limit the use of sandwich construction in aircraft structural elements. Results of fatigue tests showed no discernible effect from the level of damage, at least to 60,000 cycles.

Tests run on specimens with ultrasonically detectable, but not visually detectable damage, showed no effect on fatigue life for 1 in. (25.4 mm) radius induced damage; but two specimens, with 1/4 in. (6.4 mm) radius indenter induced damage, failed in fatigue. Again, failures were compressive buckled through the test section.

Specimens damaged at the visual threshold level all failed during fatigue testing, one specimen failed in as few as 9 cycles while another survived as many as 7411 cycles. Failure modes were the same as previous tests.

Figure 27 presents fatigue life versus indention from the above tests, with the results for those specimens which failed statically (upon initial load application) shown to have a life of 0.5 cycles or less each. Because of the large scatter in this data, only qualitative conclusions can be drawn.

The results tend to support the equivalence of static to dynamic damage. Indentations of up to .030 in. (.76 mm) for the 1/4 in. (6.4 mm) radius indenter and up to .045 in. (1.14 mm) for the 1 in. (25.4 mm) radius indenter do not affect the fatigue life. These indentations correspond to ultrasonically detectable damage areas of equivalent diameter of .45 in. (11.5 mm) for the 1/4 in. (6.4 mm) radius indenter and .60 in. (15.2 mm) equivalent diameter for the 1 in. (25.4 mm) radius indenter based on the indentation versus damage area curve, Figure 11.

Fatigue tests were conducted on specimens with impact damage less than readily visible but above the visual threshold to determine the maximum strain level the subject sandwich structure can tolerate in service and still suffer no degradations due to the greatest damage which would not be easily seen and therefore not immediately repaired. From the results of these tests as presented in Figure 28 (Table III specimens 33 thru 39), it is seen that these visually damaged specimens can withstand fatigue cycling to a strain of .0033 for at least 100,000 cycles.

Current Navy design criteria for graphite/epoxy structures sets the design ultimate compression strain at .0050 for laminates with 1/4 in. (6.4 mm) diameter manufactured holes. This results in a design limit strain of .0033, equal to the maximum reference strain determined above. Thus designs which compensate for the inclusion of fastener holes should also accommodate visual threshold impact damage.

It is interesting to note that the effects of the damage caused by the .696 lb (316 g), 1/4 in. (6.4 mm) radius indenter impacting the sandwich beam at 20 ft/sec (6.1 m/s) on compressive fatigue life is roughly equivalent to the effects of the 1.5 lb (680 g), 1 in. (25.4 mm) radius indenter impacting the beam at the same speed.

The four-point-bending test fixture used in the previous tests imposes a load state on the sandwich beam which would be encountered on secondary structures such as flaps, spoilers, elevators, etc. In these cases, the sandwich is loaded by bending so that the upper and lower faces are stressed oppositely. This is considered a severe test since failure of one face destablizes the structure. Uniaxial in-plane compression, with both faces loaded the same, would allow the load to transfer by shear through the core from the damaged face to the undamaged

face. It was postulated that the effect of damage would therefore not be as great. A structural example of sandwich panels under such uniaxial type loading is fuselage skins.

Four sandwich beams were impact damaged and subsequently fatigue tested in uniaxial compression at R = $-\infty$ in a 100 KIP MTS fatigue machine to determine if there was a difference in the fatigue life of the damaged face sheet when compared with results of identically damaged panels in four-point-bending fatigue tests. An undamaged specimen was also tested. Results are presented in Table IV and in Figure 28. It is seen that fatigue life of the damaged specimens during the uniaxial fatigue test is below that determined from the four-point-bending fatigue tests. The reason for this difference is discussed in the next section.

DAMAGE GROWTH

Of the 39 specimens fatigue tested under four-point-bending, only in 7 cases was damage growth observed; see Table III specimens 14 through 17, 29, 35 and 36. Where growth was noted, it usually occurred within the first 2000 cycles, after which no additional growth was noted, even though in one case the specimen failed 6000 cycles later. Of the total of 14 specimens which failed in fatigue only 2, specimens 16 & 36, had any observed damage growth prior to failure. Damage growth consisted of a slight increase in the ultrasonic detectable damage region and/or minor delamination of the surface ply. In general, though, the size of damage did not grow with cycling, although there may be a weakening of the matrix around the damage region and/or a growth of damage within the initial damage region which contributes to eventual failure.

The results of the uniaxial compression fatigue tests were in sharp contrast to those of the four-point-bend fatigue tests. Dramatic delamination of the surface 0° ply was observed in uniaxial testing on the damaged face sheet. Static strength of a damaged sandwich panel in uniaxial compression was also less than a similarly damaged sandwich panel in the four-point-bend test. Table IV summarizes the results of the uniaxial compression fatigue tests and Figure 29 traces the growth of the surface ply delamination for one specimen. It can be concluded that the effect of cycling tended to reduce the stress concentration, as two specimens which had been cycled at strains below that of the static failure point were then able to withstand limited cycling above the static failure strain.

The reason for the difference in damage growth between uniaxial and four-point-bend tests is attributed to the curvature of the sandwich face imposed by the bending test which constrains the 0° surface ply in the direction normal to the face and prevents this ply from buckling upward away from the face sheet and therefore causing delamination. The uniaxial loading imposes no such constraint, Figure 30. Reference 6 observed that the use of a 0° ply as the outside layer causes delamination to occur much sooner than if the outer plies were $\pm 45^{\circ}$. According to reference 6, it was uncertain if the reason for the matrix failure resulting in the delamination results from the cycling of the interlaminar shear stress, the tensile stress normal to the face or a combination of both. The results of this work suggests the delamination results from the tensile stress normal to the face.

CONCLUSIONS

1. A method which employs static tests to simulate impact damage of a graphite-epoxy sandwich structure has been developed and validated.

2. For graphite-epoxy structures, impact damage which is not visually detectable can degrade structural properties, although designs which compensate for the use of fastener holes will also accommodate visual threshold impact damage.

3. For graphite-epoxy structures, ultrasonic pulse-echo inspection will detect impact damage which degrades structural properties.

4. Failures in graphite/epoxy sandwich structures with impact damage are associated with crippling of the core which results in higher bending stress in the face sheet, and delamination of the face sheet, both of which contribute to ultimate buckling failures in compression.

5. Indenter radius is an important parameter in influencing impact damage of graphite-epoxy structures.

RECOMMENDATIONS

1. Gr/Ep structures subject to impact threats should be designed to reduced strain allowables to compensate for possible impact damage. An approach could be to require a design to be able to tolerate a 1/4 in. (6.4 mm) diameter hole at any location on the surface of the structure.

2. An impact damage indicator system should be developed. This could be a permanent coating applied to the surface of the structure which would change color upon a structurally degrading impact.

3. A core material for graphite-epoxy sandwich structures should be developed which would absorb more loading normal to the face sheet before crippling.

4. Lamination sequences used in graphite/epoxy sandwich skins incorporating $\pm 45^{\circ}$ outer plies seem desirable.

REFERENCES

1. Rhodes, M. D., "Low Velocity Impact on Composite Sandwich Structures", presented at the Second Air Force Conference on Fibrous Composites in Flight Vehicle Design, Dayton, Ohio, 22-24 May 1974.

2. Rhodes, M. D., "Impact Fracture of Composite Sandwich Structures", presented at the ASME/AIAA/SAE 16th Structures, Structural Dynamics, and Materials Conference, Denver, Colorado, 27-29 May 1975.

3. Slepetz, J. M., Oplinger, D. W., Parker, B. S., and Tremblay, R. T., "Impact Damage Tolerance of Graphite/Epoxy Sandwich Panels", AMMRC TR 74-20, Sep 1974.

4. Adsit, N. R. and Waszczak, J. P., "Investigation of Damage Tolerance of Graphite/Epoxy Structures and Related Design Implications," Naval Air Development Center Report Number NADC-76387-30.

5. Chou, P. C., and Flis, W. J., "Design Curves for Structural Response Due to Impact Loading", Naval Air Development Center Report Number NADC-76380-30, October 1976.

6. Rosenfeld, M. S. and Huang, S. L., "Fatigue Characteristics of Graphite/Epoxy Laminates Under Compression Loading" presented at the AIAA/ASME 18th Structures, Structural Dynamics & Materials Conference, San Diego, CA, 21-23 March 1977.

Table 1 - Damage Resulting from Static Indentation Tests

1.0 in. = 25.4 mm

Specimen	Indenter Radius (in)	Indentation Depth (in)	Visually Detected Damage			Ultrasonically Detected Damage		
			Length (in)	Width (in)	Depth (in)	Length (in)	Width (in)	Area (in^2)
1	1	.110			.004	1.12	1.20	1.056
2	1	.106			.010	1.00	.80	.628
3	1	.138	.90	.70	.018	1.45	.82	.934
4	.25	.153	.58	.45	.048	.75	.70	.412
5	.25	.154	.60	.42	.054	.65	.58	.296
6	.25	.154	.60	.45	.042	.78	.65	.398
7	.25	.0324				.44	.22	.076
8	.25	.0144				.25	.25	.049
9	.25	.0156				.25	.25	.049
10	1	.02						0
11	1	.012						0
12	1	.016						0
13	1	.029				.44	.25	.086
14	1	.0325				.50	.38	.149
15	1	.028				.44	.44	.152
16	.25	.033			.002	.59	.44	.204
17	.25	.032			.002	.59	.50	.232
18	.25	.032			.002	.56	.53	.233
19	.25	.061	.34	.22	.011	.80	.55	.346
20	.25	.053	.26	.18	.007	.80	.55	.346
21	.25	.062	.30	.22	.011	.82	.45	.290
22	1	.062			.005	.90	.75	.530
23	1	.070			.004	.80	.80	.503
24	1	.065			.004	.75	.82	.483

Table II - Damage Resulting from Dropped Weight Impact Tests

Drop Height = 6.211 ft (1.89 m)

Spec No.	Indenter Radius (in)	Indenter Mass (Lbm)	Calculated Indentation Depth (in)	Visually Detectable Damage			Ultrasonic Damage		
				Length (in)	Width (in)	Depth (in)	Length (in)	Width (in)	Area (in^2)
25	1	.220	.043				.75	.50	.295
26	1	.800	.093	.42	.46	.007	1.20	.86	.811
27	1	1.50	.126	.70	.80	.015	1.68	1.38	1.821
28	1	.500	.065			.003	1.00	.82	.644
29	.25	.110	.028				.45	.32	.113
30	.25	.246	.051			.003	.65	.51	.260
31	.25	.386	.067	.30	.30	.017	.68	.55	.294
32	.25	.696	.147	.60	.45	.119	.74	.79	.459
33	1	.500	.065			.002	.90	.80	.565
34	.25	.386	.067	.38	.28	.014	.70	.55	.302
35	.25	.386	.067	.38	.30	.009	.67	.52	.274
36	1	1.50	.126	.80	.70	.018	1.70	1.20	1.60
37	1	1.50	.126	.90	.54	.011	1.50	1.00	1.18
38	.25	.696	.147	.70	.50	.086	.86	.79	.53
39	.25	.696	.147	.58	.45	.120	.72	.83	.47
40	.25	.696	.147	.70	.45	.089	1.02	.80	.64
41	.25	.696	.147	.60	.45	.115	.95	.72	.54
42	.25	.696	.147	.55	.45	.076	1.00	.75	.59
43	.25	.696	.147	.54	.42	.090	.94	.85	.63

1.00 in. = 25.4 mm
1.0 Lbm = 454 g

Table III - Four Point Bending Fatigue Test Results

$R = -\infty$, Frequency = 1.25 HZ

Specimen	Indenter Radius	Indentation (in)	Max. Comp. Strain % (5930×15^6)	Cycles to Failure	Comments
Control	-	-	100	100000+	
1	1	.110	65		Static Failure
2	1	.106	96		Static Failure
3	1	.138	81		Static Failure
4	.25	.153	79		Static Failure
5	.25	.154	100		Static Failure
6	.25	.154	75		Static Failure
7	.25	.0324	100	6433	
8	.25	.0144	100	100000+	
9	.25	.0156	100	60000+	
10	1	.02	100	60000+	
11	1	.012	100	60000+	
12	1	.016	100	60000+	
13	1	.029	100	100000+	
14	1	.0325	100	87000+	Damage growth at 2000 cycles ΔLength = 0 ΔWidth = .06
15	1	.028	100	60000+	Damage growth at 2000 cycles ΔLength = .06 ΔWidth = 0
16	.25	.033	100	8266	Damage growth at 2000 cycles ΔLength = 0 ΔWidth = .03
17	.25	.032	100	60000+	Damage growth at 2000 cycles ΔLength = .06 ΔWidth = 0
18	.25	.032	100	60000+	
19	.25	.061	97		Static Failure
20	.25	.053	100	34	
21	.25	.062	100	2	
22	1	.062	100	9	
23	1	.070	100	3460	
24	1	.065	100	494	
25	1	.043	100	60000+	
26	1	.093	82		Static Failure
27	1	.126	72		Static Failure
28	1	.065	100	1113	
29	.25	.028	100	60000+	Damage growth at 20,000 cycles ΔLength = .05 ΔWidth = .05
30	.25	.051	100	7411	

Table III - Four Point Bending Fatigue Test Results (Cont.)

Specimen	Indenter Radius	Indentation (in)	Max. Comp. Strain % (5930×15^6)	Cycles to Failure	Comments
31	.25	.067	100	5	
32	.25	.147	74		Static Failure
33	1	.065	80	60000+	
34	.25	.067	80	1894	
35	.25	.067	60	60000+	NDI Damage Growth ΔLength = .14 ΔWidth = 0
36	1	.126	60	4516	Damage growth at 2000 cycles surface ply delamination ΔLength = 0 ΔWidth = .2
37	1	.126	65	66	
38	.25	.147	60	60000+	
39	.25	.147	65	965	

Table IV - Uniaxial Compression Fatigue Test Results

R = -∞ , Frequency = 1.25 HZ 1.00 in. = 25.4 mm

Specimen	Indenter Radius (in)	Indentation (in)	Max. Comp. Strain	Cycles To Failure	Comments
Control			5723	100000+	
40	1/4	.147	3679		Static failure
41	1/4	.147	2861	60000+	Damage growth after 10000 cycles ΔA = 0 ΔB = .08 Additional growth after 20000 cycles ΔA = .06 ΔB = .15
			4000	25	Retest at higher strain Damage growth upon first cycle ΔA = 0 ΔB = .55 Delamination of surface ply
42	1/4	.147	3262	102000+	Damage growth upon load growth delamination of surface ply Damage growth after 100 cycles ΔA = 0 ΔB = .44 Additional growth after 22000 cycles ΔA = 0 ΔB = .20 Additional growth after 42000 cycles ΔA = 0 ΔB = .31
43	1/4	.147	3500	10000+	Damage growth within first 100 cycles delamination of surface ply ΔA = 0 ΔB = .34
			4000	50	Retest at higher strain No damage growth prior to failure

SANDWICH BEAM IMPACT SPECIMEN

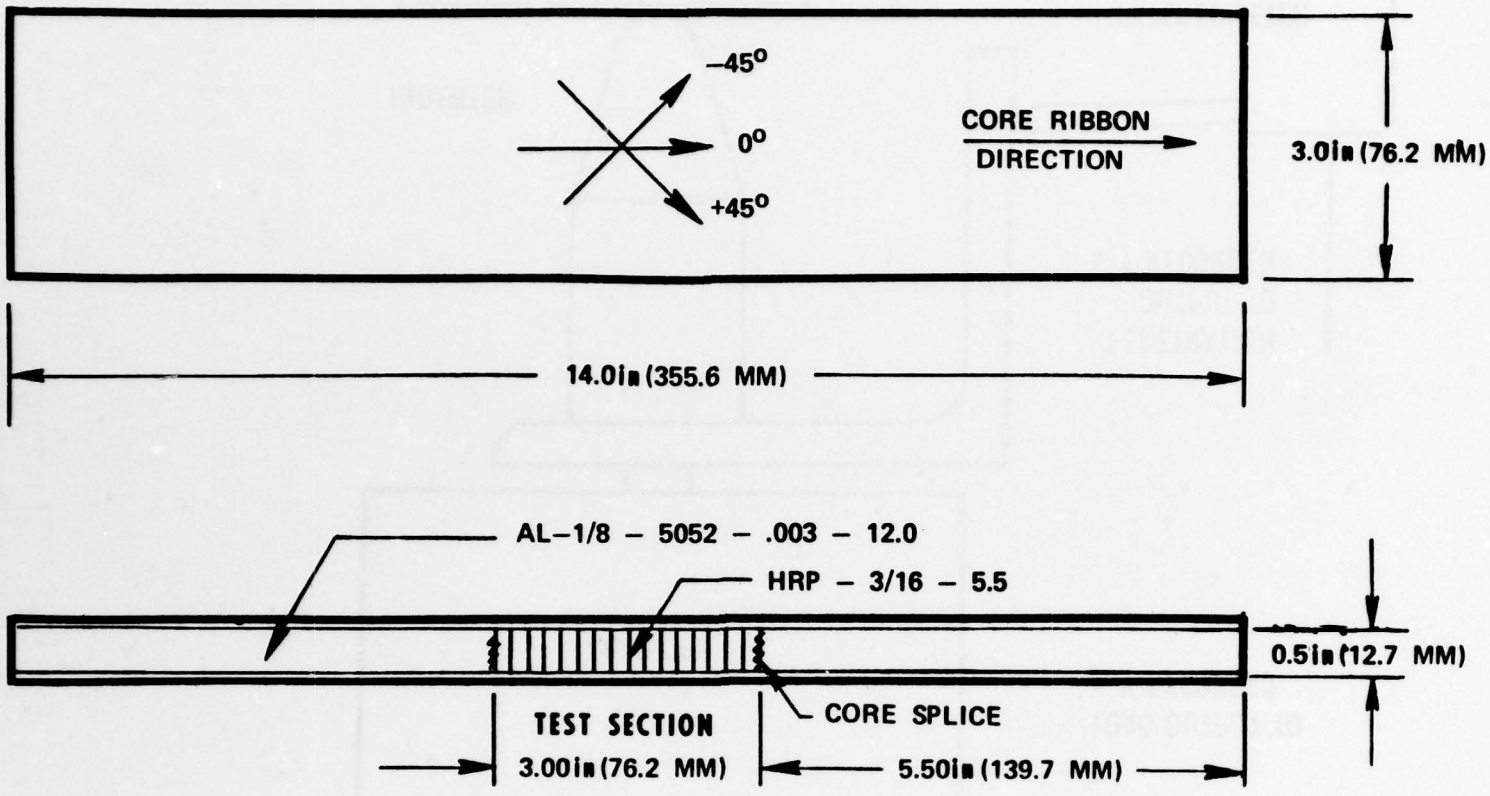

TOP FACE: $[0/\pm 45/0_2/\mp 45/0]$ AS/3501-6
ADHESIVE: FM-123-5 FILM
CORE SPLICE: 3M EC-3500 B/A
BOTTOM FACE $[0/\mp 45/0_2/\pm 45/0]$ AS/3501-6

Figure 1. Test Specimen.

NADC-77305-60

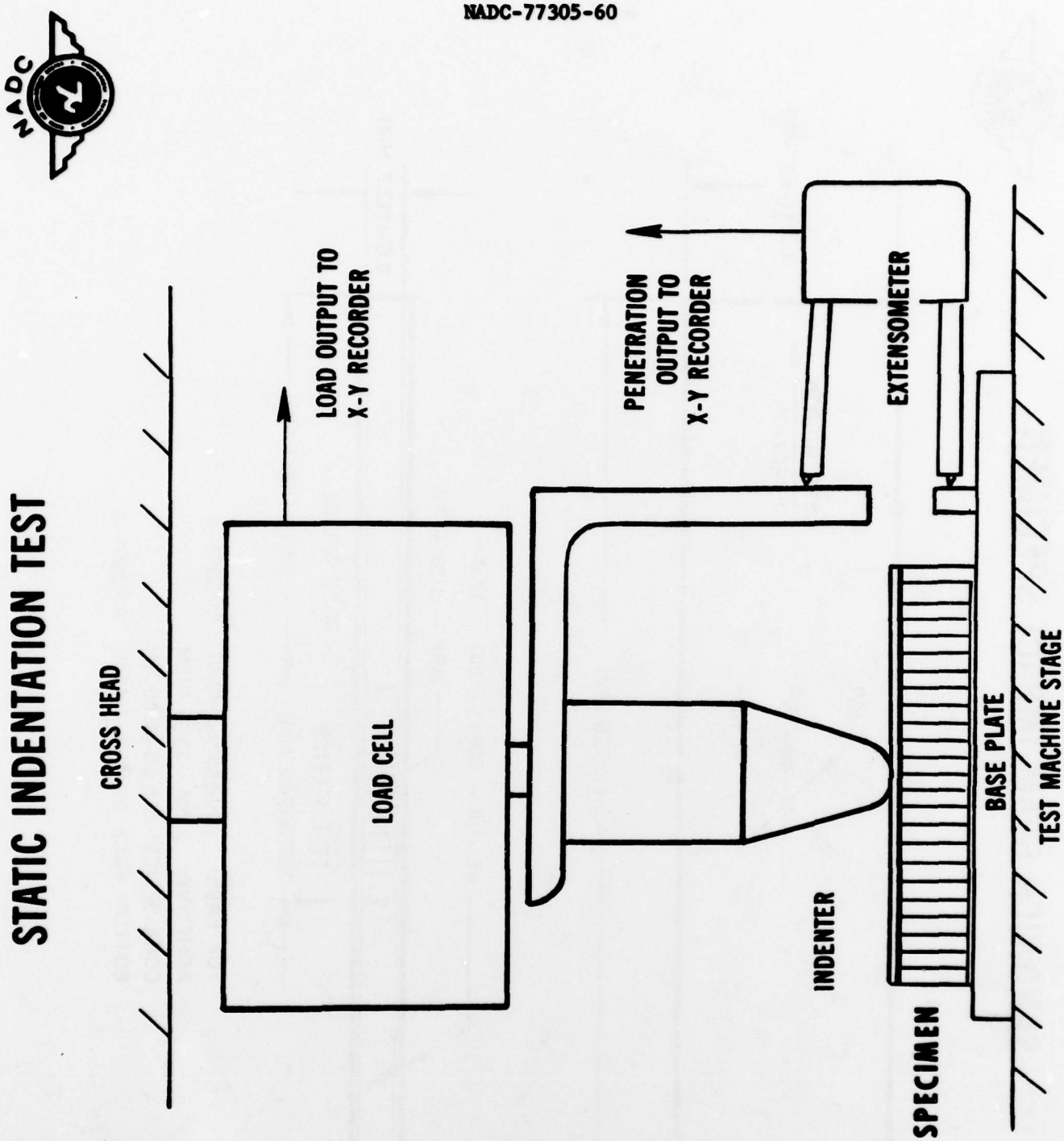

Figure 2. Static Indentation Test.

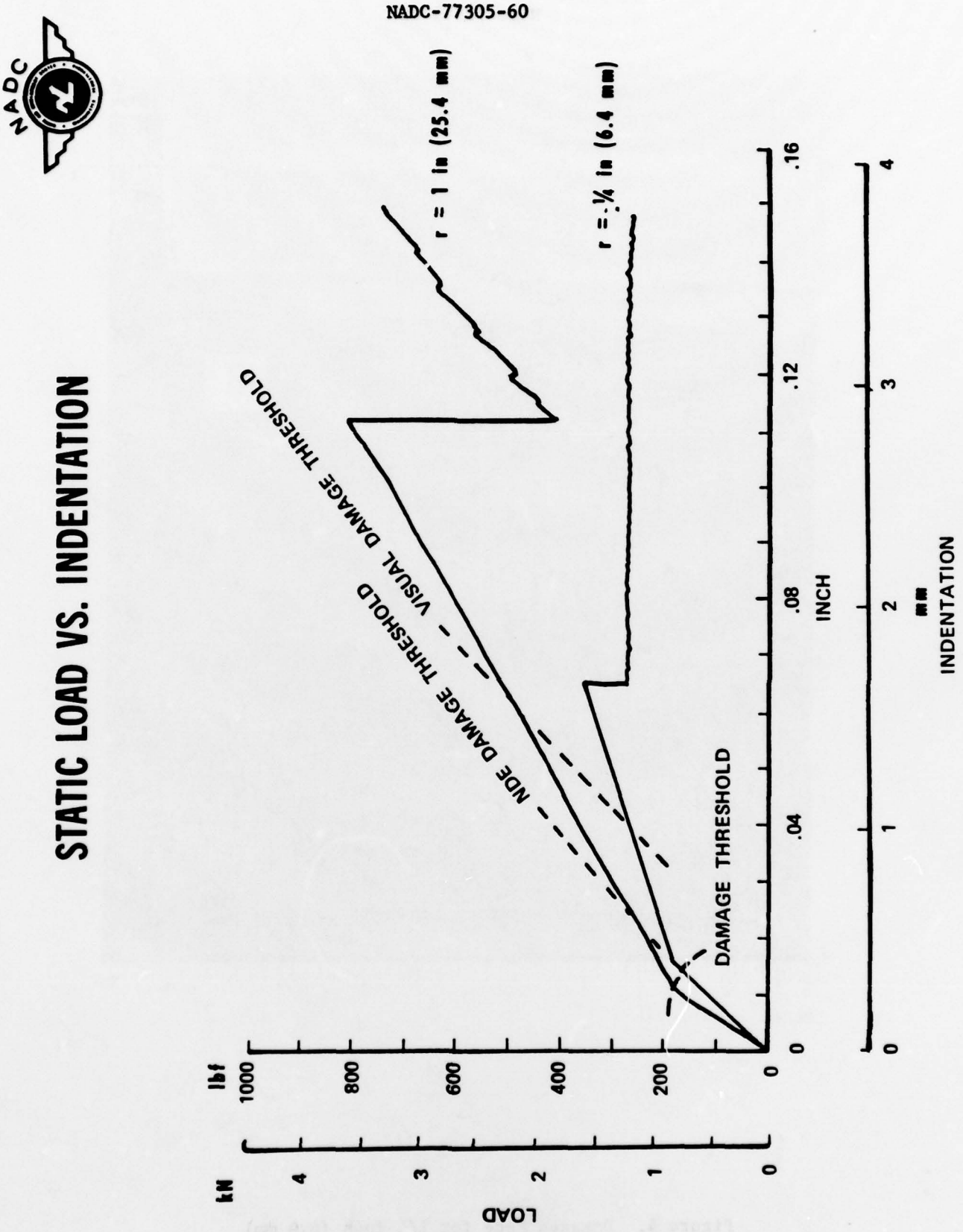

Figure 3. Load Versus Indentation From Static Test.

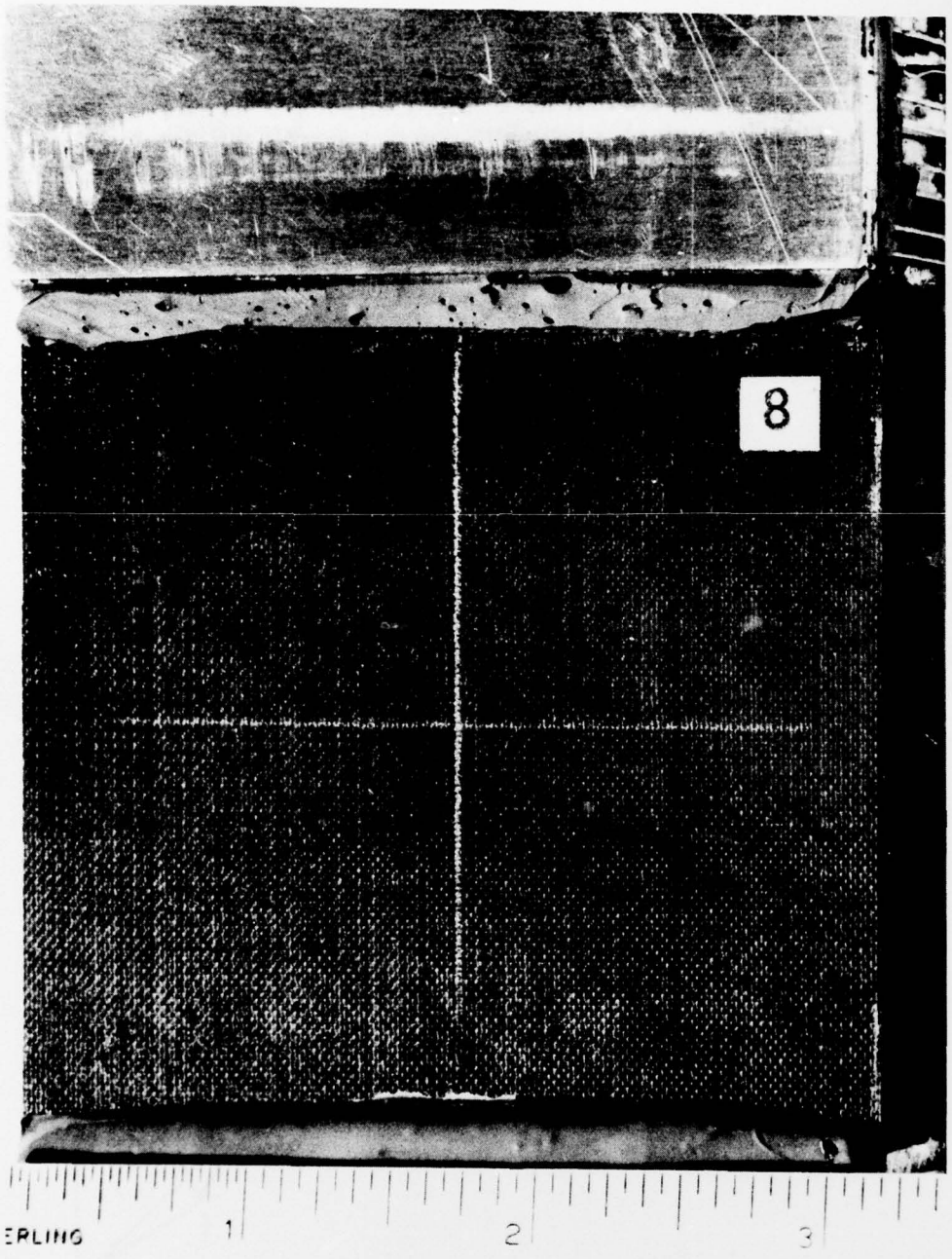

Figure 4. Damaged Face for 1/4 inch (6.4 mm)
Radius Indenter at 0.0144 inches (0.37 mm) Indentation

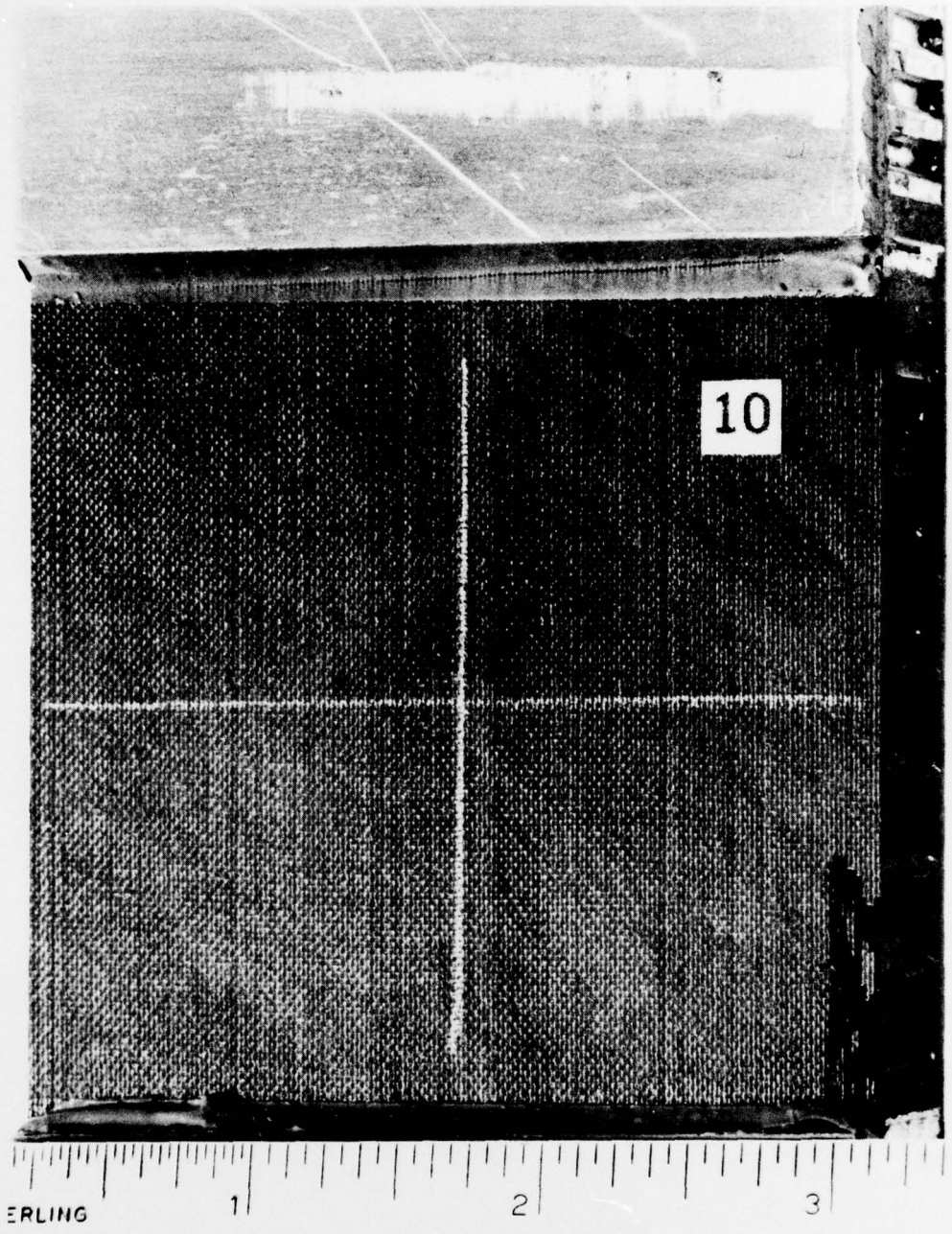

Figure 5. Damaged Face for 1 inch (25.4 mm)
Radius Indenter at 0.020 inches (0.51 mm) Indentation

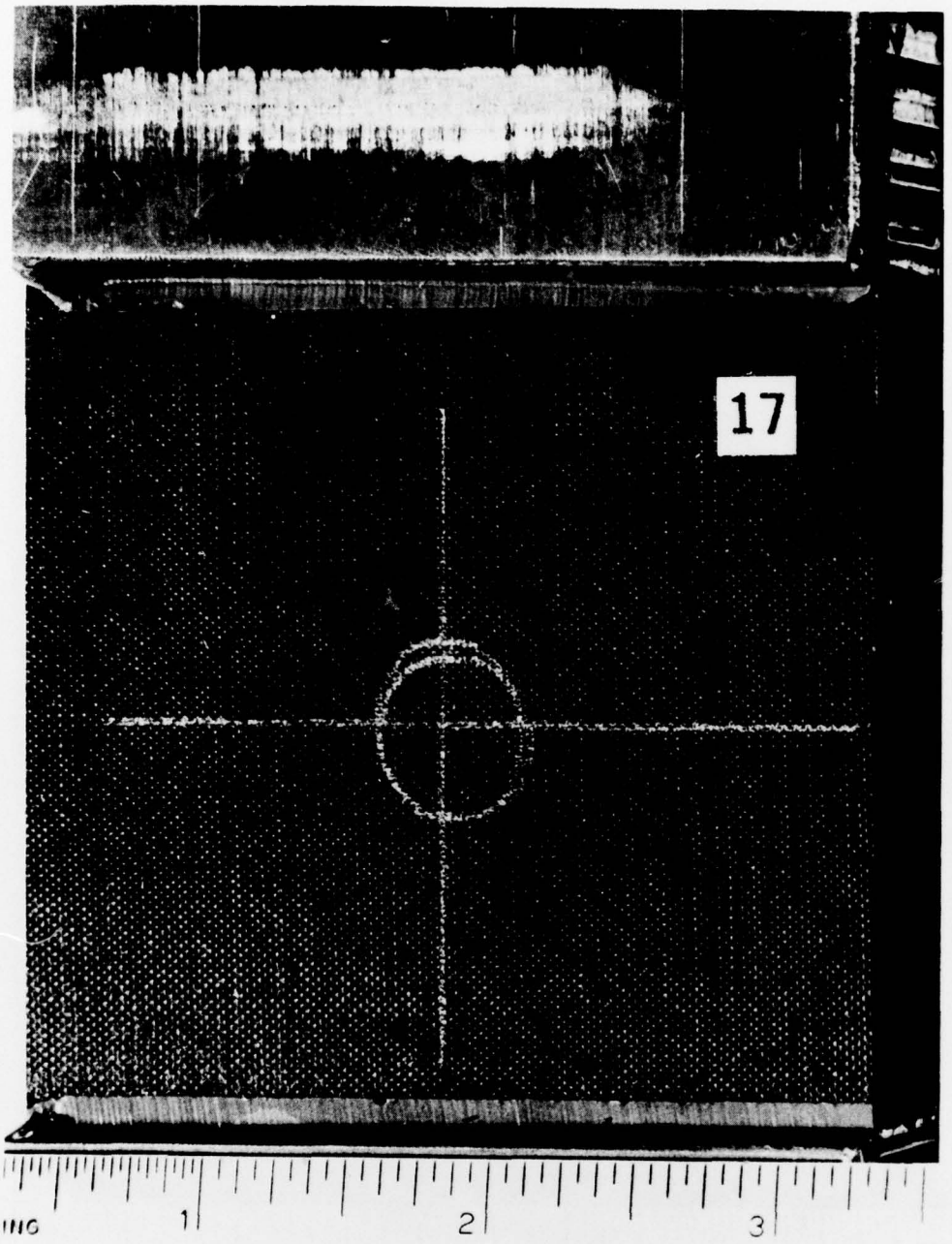

Figure 6. Damaged Face for 1/4 inch (6.4 mm) Radius Indenter at 0.032 inches (0.81 mm) Indentation. (Delamination Outlined by White Pencil Circle)

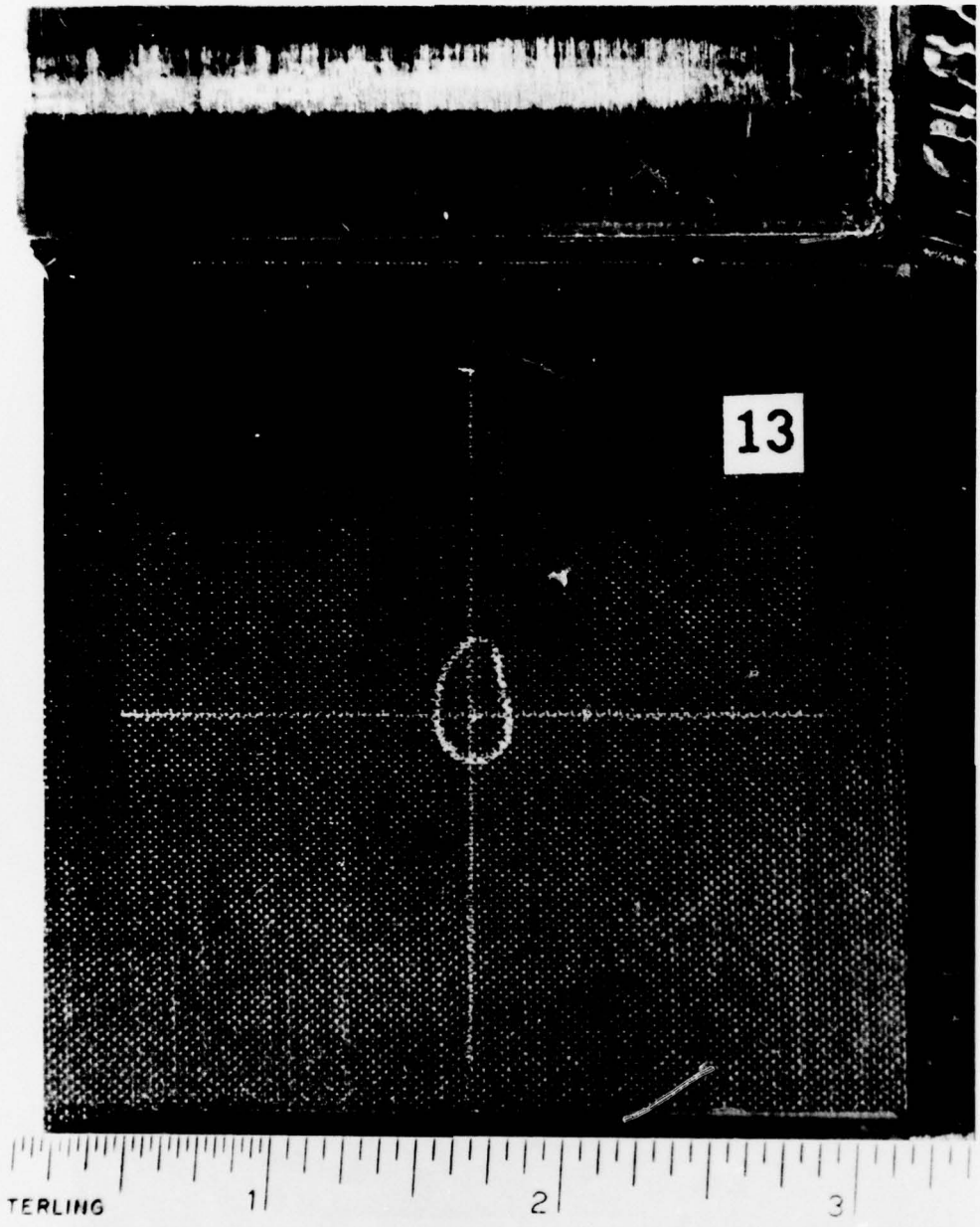

Figure 7. Damaged Face for 1 inch (25.4 mm)
Radius Indenter at .029 inches (.74 mm) Indentation.
(Delamination Outlined by White Pencil Circle)

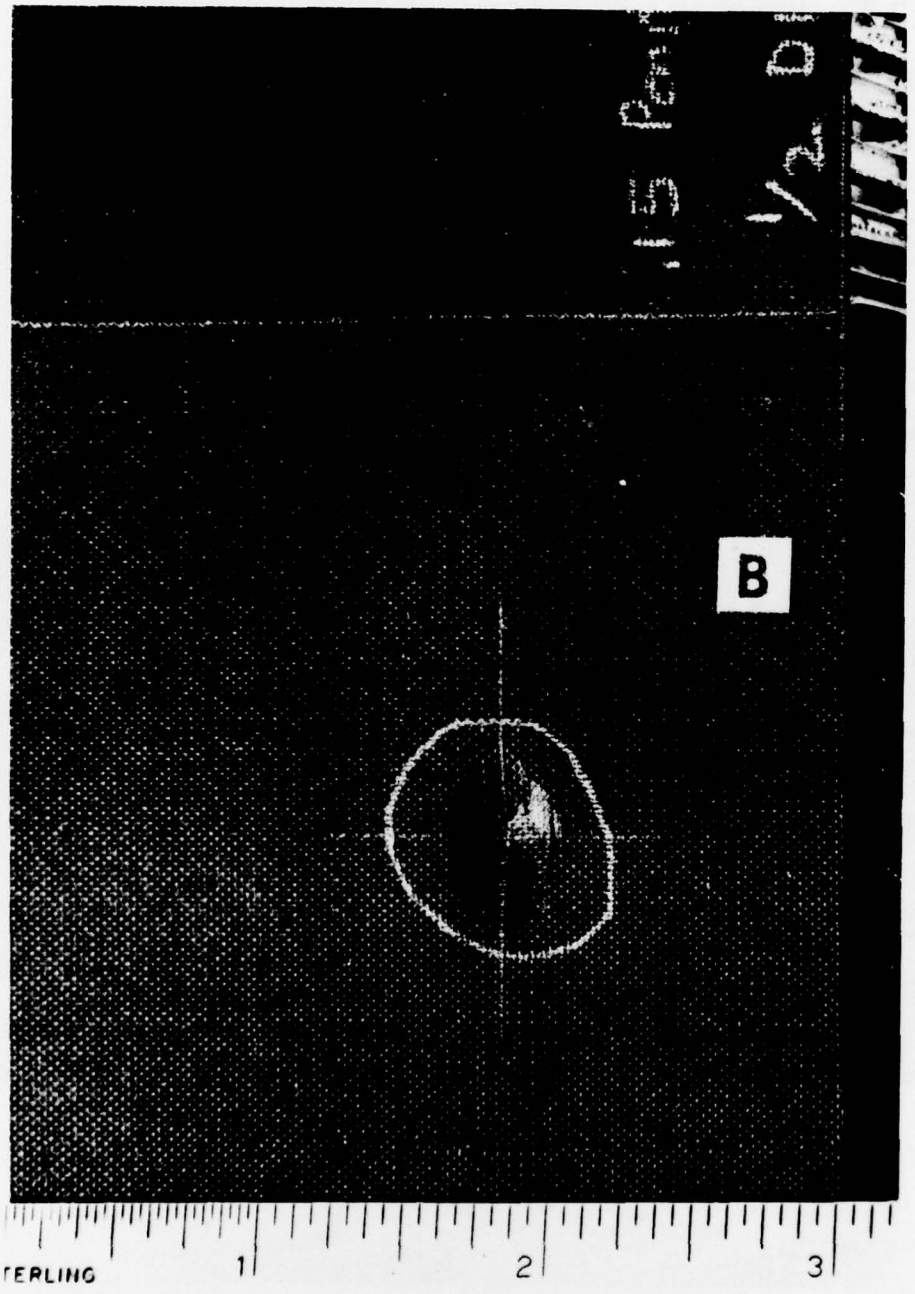

Figure 8. Damaged Face for 1/4 inch (6.4 mm) Radius Indenter at .15 inches (3.81 mm) Indentation. (Delamination Outlined by White Pencil Circle)

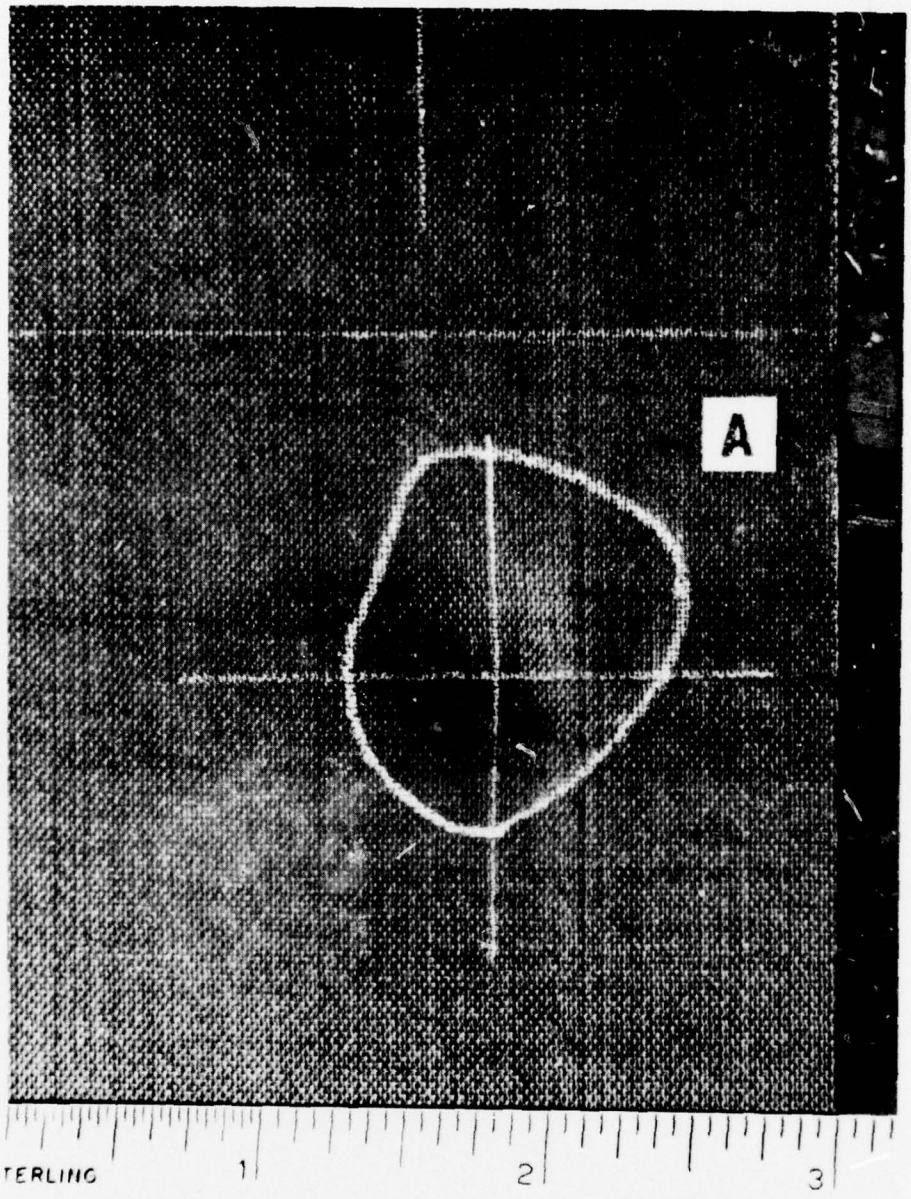

Figure 9. Damaged Face for 1 inch (25.4 mm)
Radius Indenter at .15 inches (3.81 mm) Indentation.
(Delamination Outlined by White Pencil Circle)

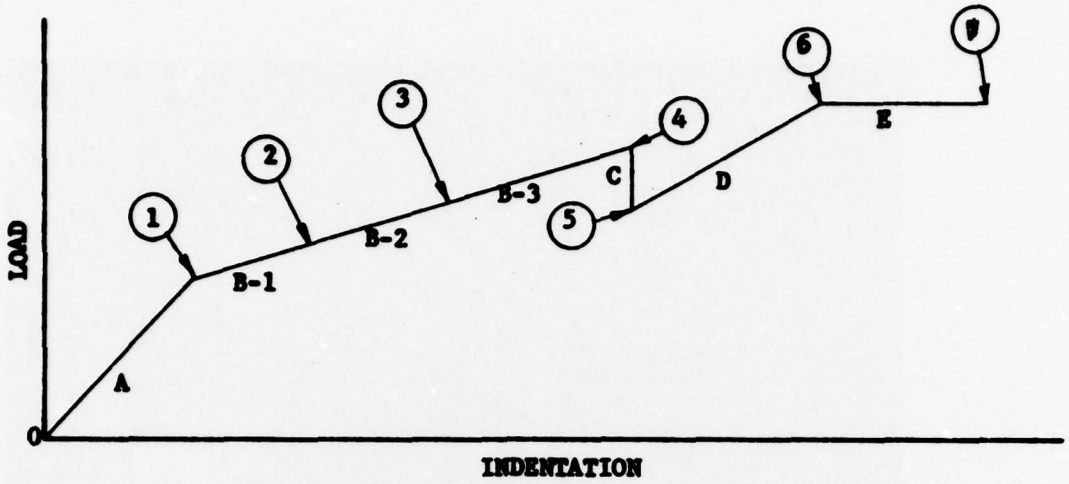

Regions

A - no damage, linear repeatable action
B-1 - damaged, undetectable visually or by UPE (Ultrasonic Pulse-Echo)
B-2 - damaged, detectable by UPE only
B-3 - damaged, detectable visually and by UPE
C - load drop with no or minute indentation increase
D - obvious damage, face sheet in bending failure and core in crushing
E - obvious damage, face sheet penetrated, core in crushing

Unique Points

1 - initiation of damage, core crushing only
2 - initiation of UPE detectable damage, of face sheet
3 - initiation of visually detectable damage of face sheet
4 - initiation of obvious face sheet damage
5 - initiation of load increase after sheet failure
6 - penetration of face sheet
7 - test end at predetermined maximum indentation

Figure 10. Idealized Load vs. Indentation Results for Static Test.

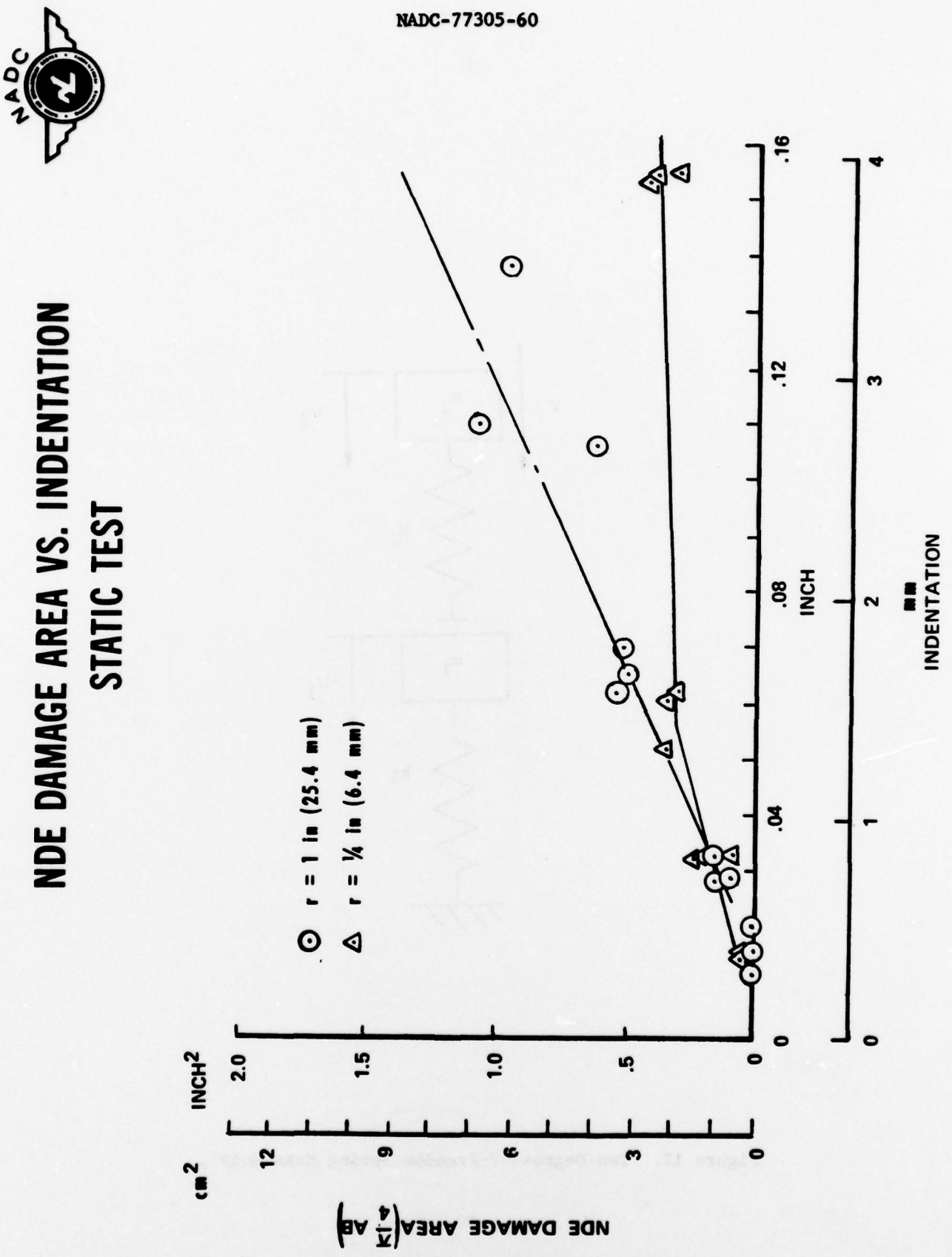

Figure 11. Damage Area Versus Indentation From Static Test.

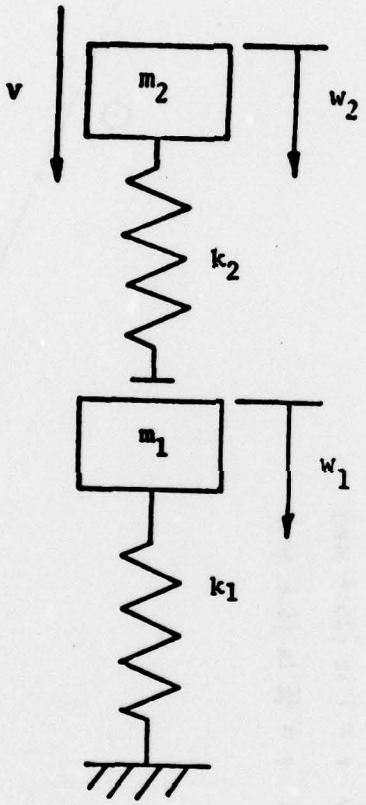

Figure 12. Two-Degree-of-Freedom Spring Mass Model.

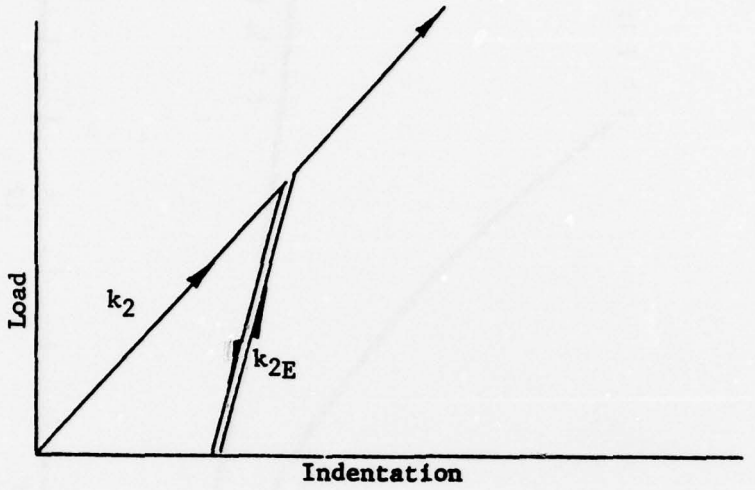

Figure 13. Plastic Elastic Load Indentation Curve

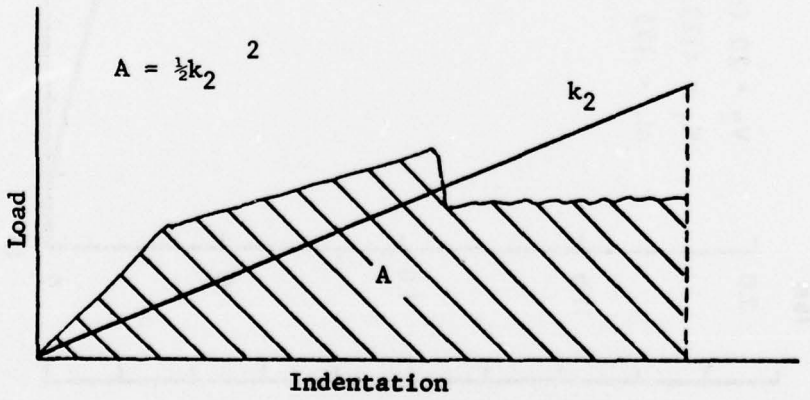

Figure 14. Approximation of k_2 from Actual Load-Indentation Curve.

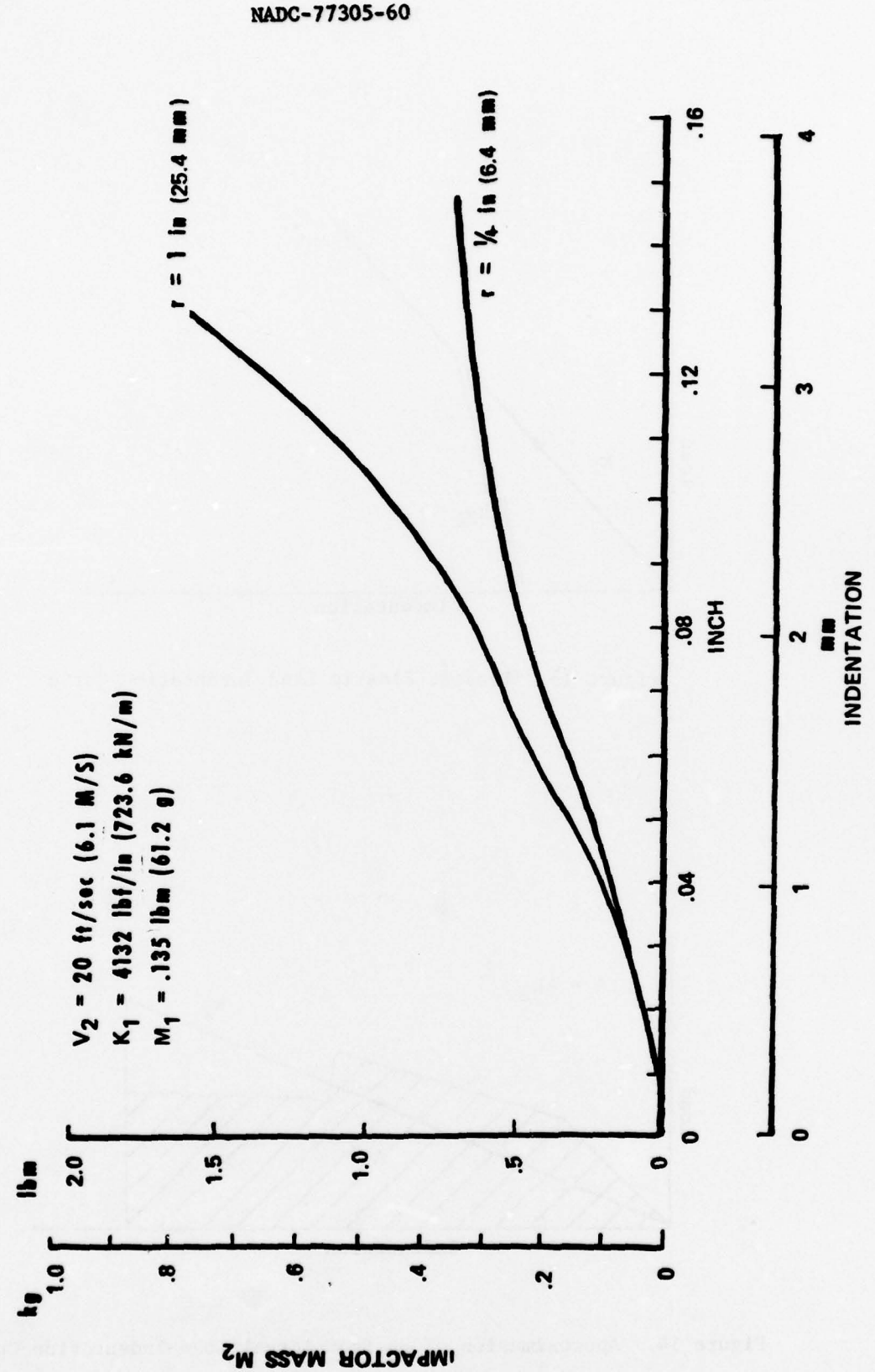

Figure 15. Indentation Versus Impact Mass for 20 ft/sec (6.1 m/s) Impact From 2 Degree-of-Freedom Analysis

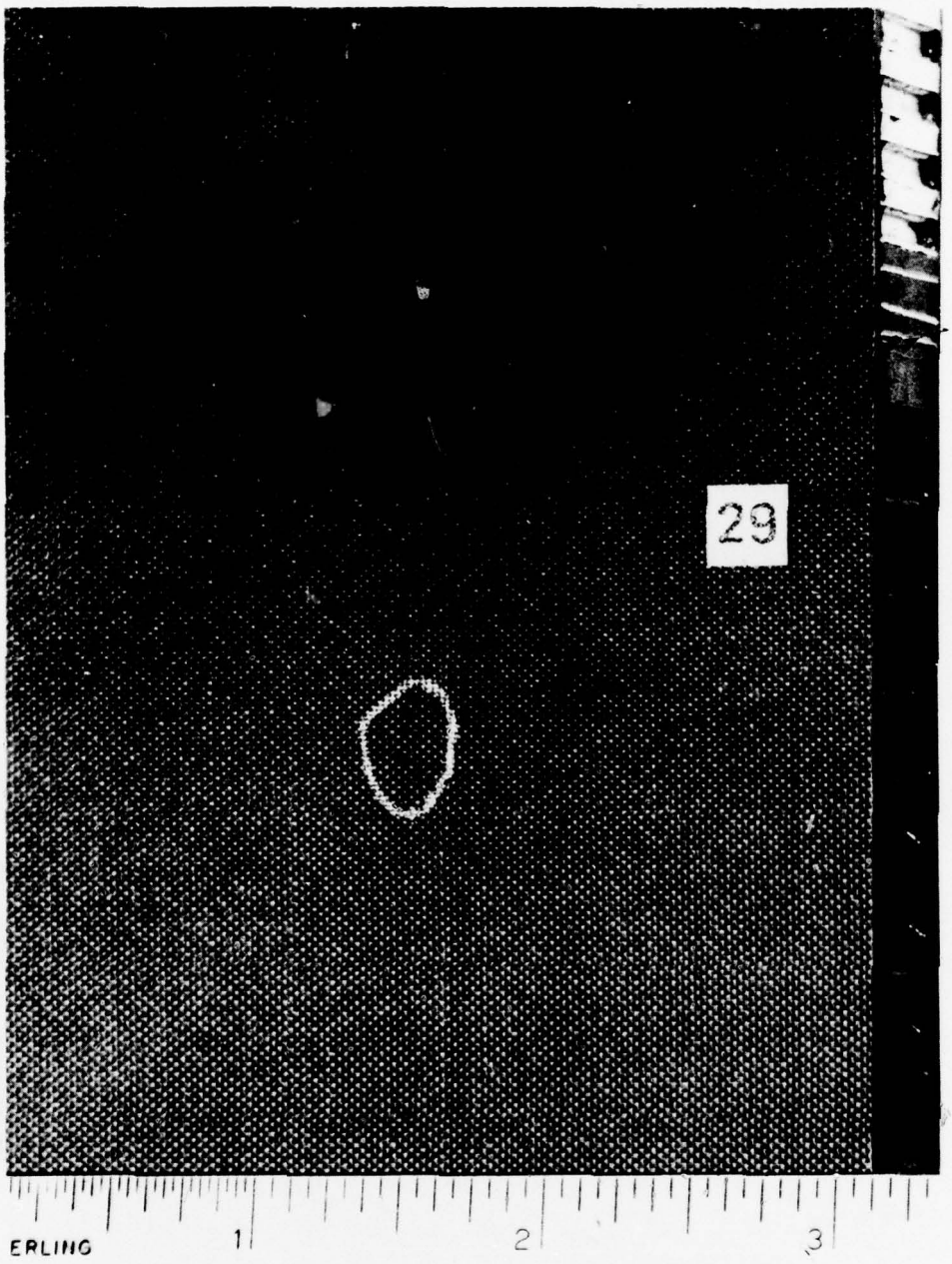

Figure 16. Damage Face for 1/4 inch (6.4 mm) Radius Indenter Impact of 0.110 lbm (49.9 g) at 20 ft/sec (6.1 m/s). (Delamination Outlined by White Pencil Circle)

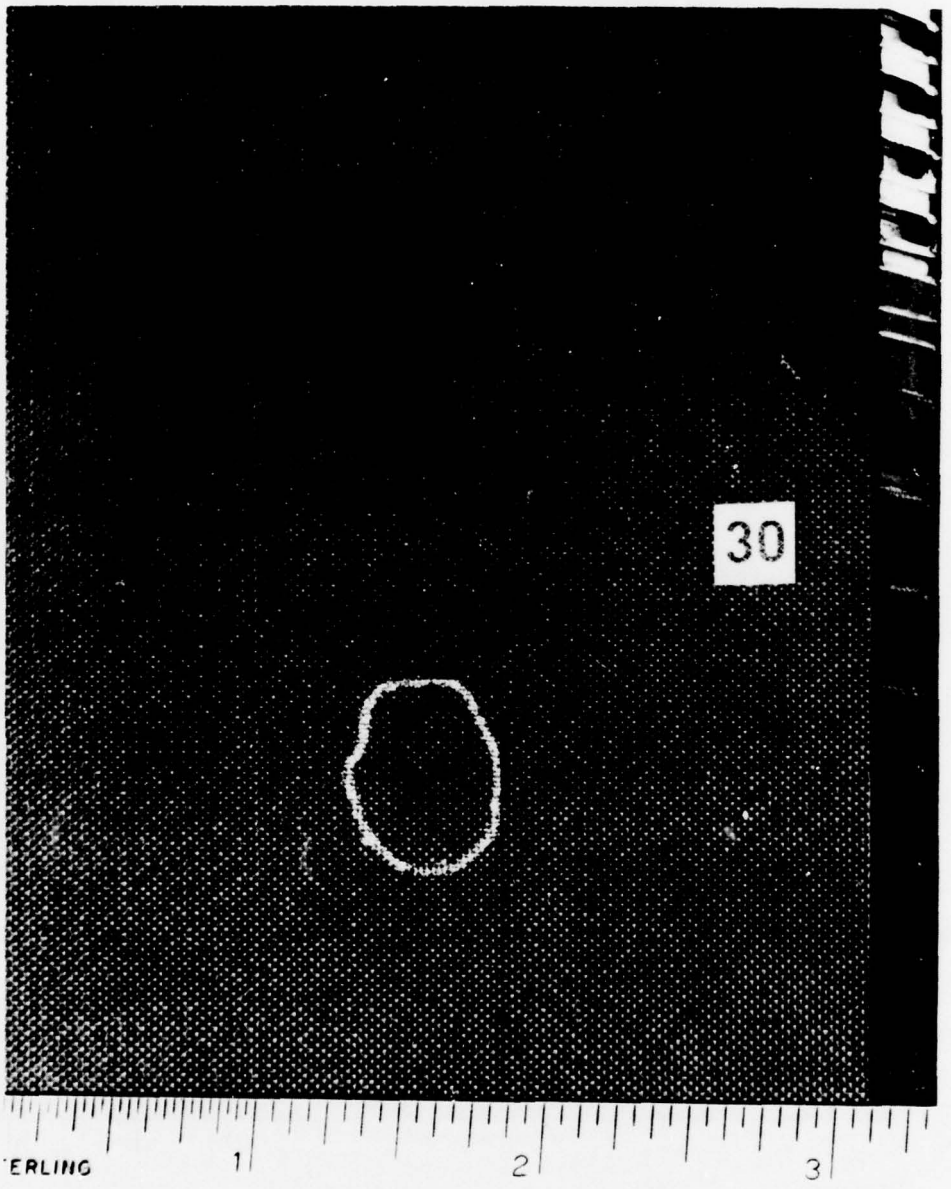

Figure 17. Damage Face for 1/4 inch (6.4 mm) Radius Indenter Impact of 0.246 lbm (111.6 g) at 20 ft/sec (6.1 m/s). (Delamination Outlined by White Pencil Circle)

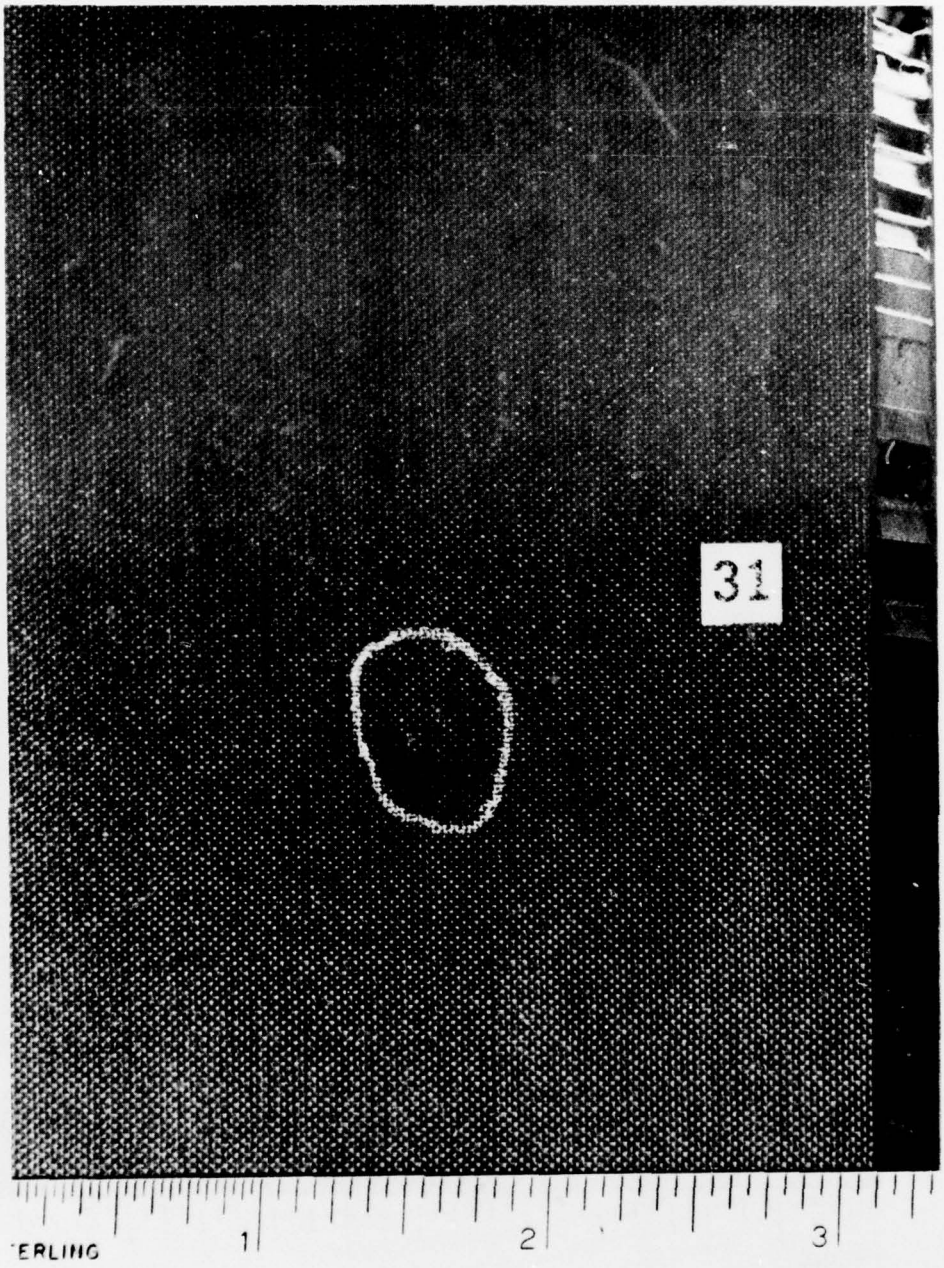

Figure 18. Damage Face for 1/4 inch (6.4 mm) Radius Indenter Impact of 0.386 lbm (175.1 g) at 20 ft/sec (6.1 m/s). (Delamination Outlined by White Pencil Circle)

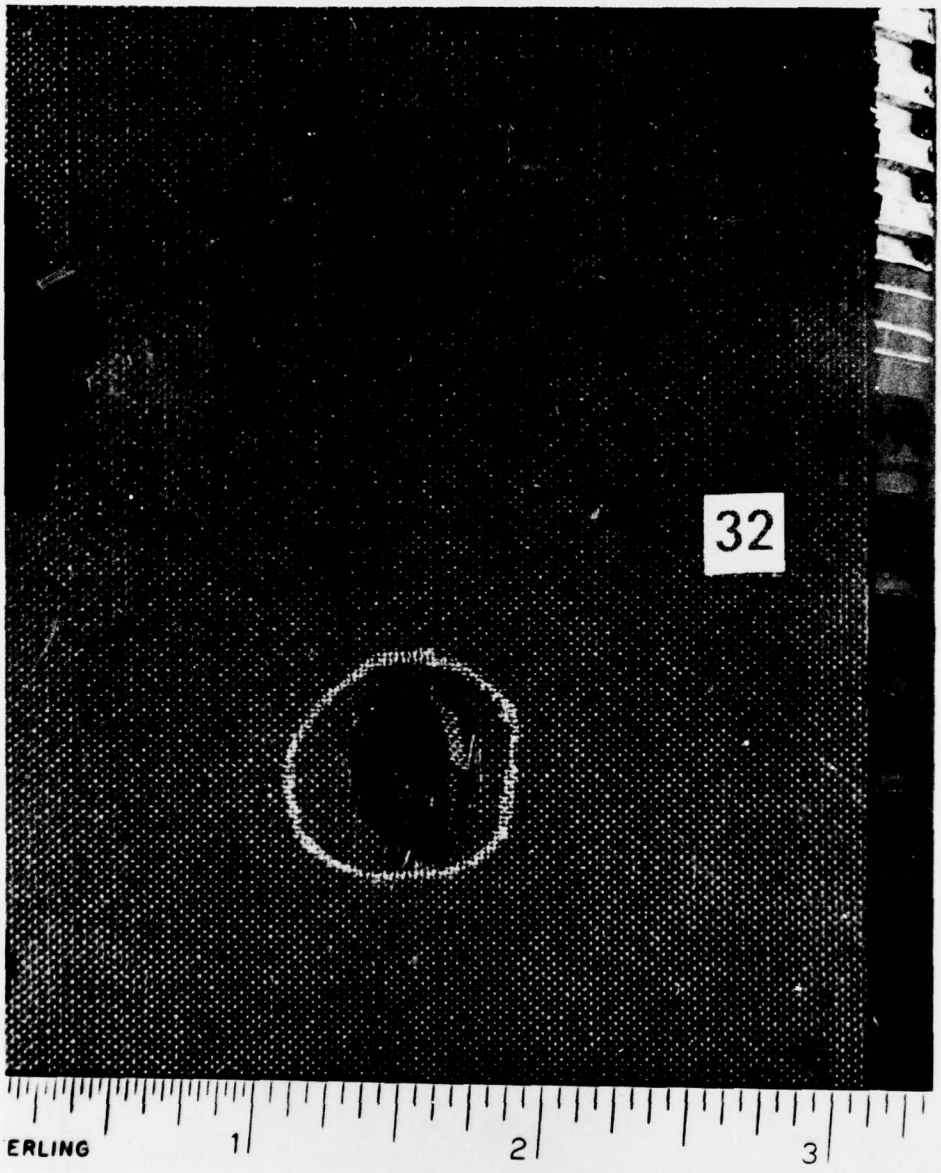

Figure 19. Damage Face for 1/4 inch (6.4 mm) Radius Indenter Impact of 0.696 lbm (315.7 g) at 20 ft/sec (6.1 m/s). (Delamination Outlined by White Pencil Circle)

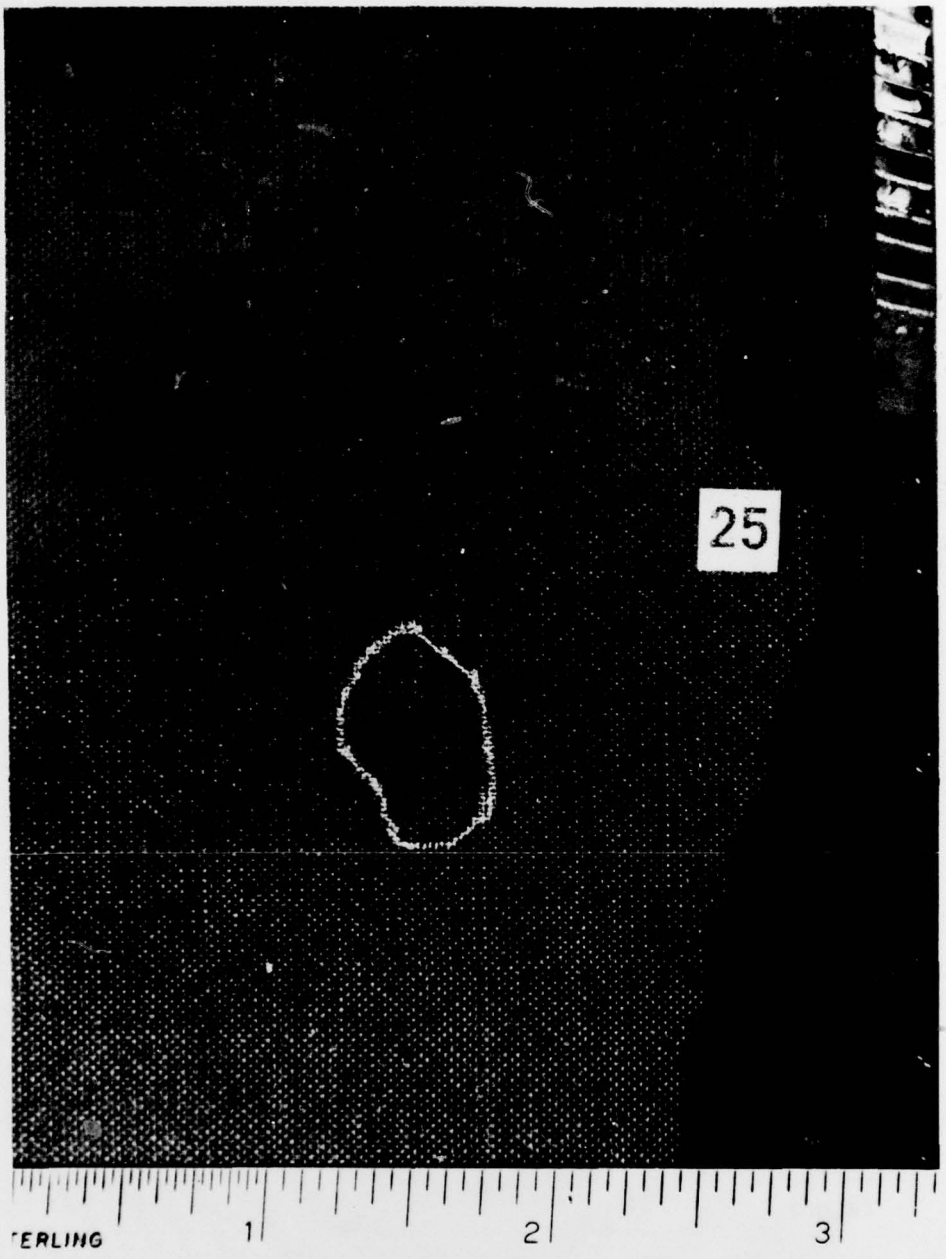

Figure 20. Damage Face for 1 inch (25.4 mm) Radius Indenter Impact of 0.220 lbm (99.8 g) at 20 ft/sec (6.1 m/s). (Delamination Outlined by White Pencil Circle)

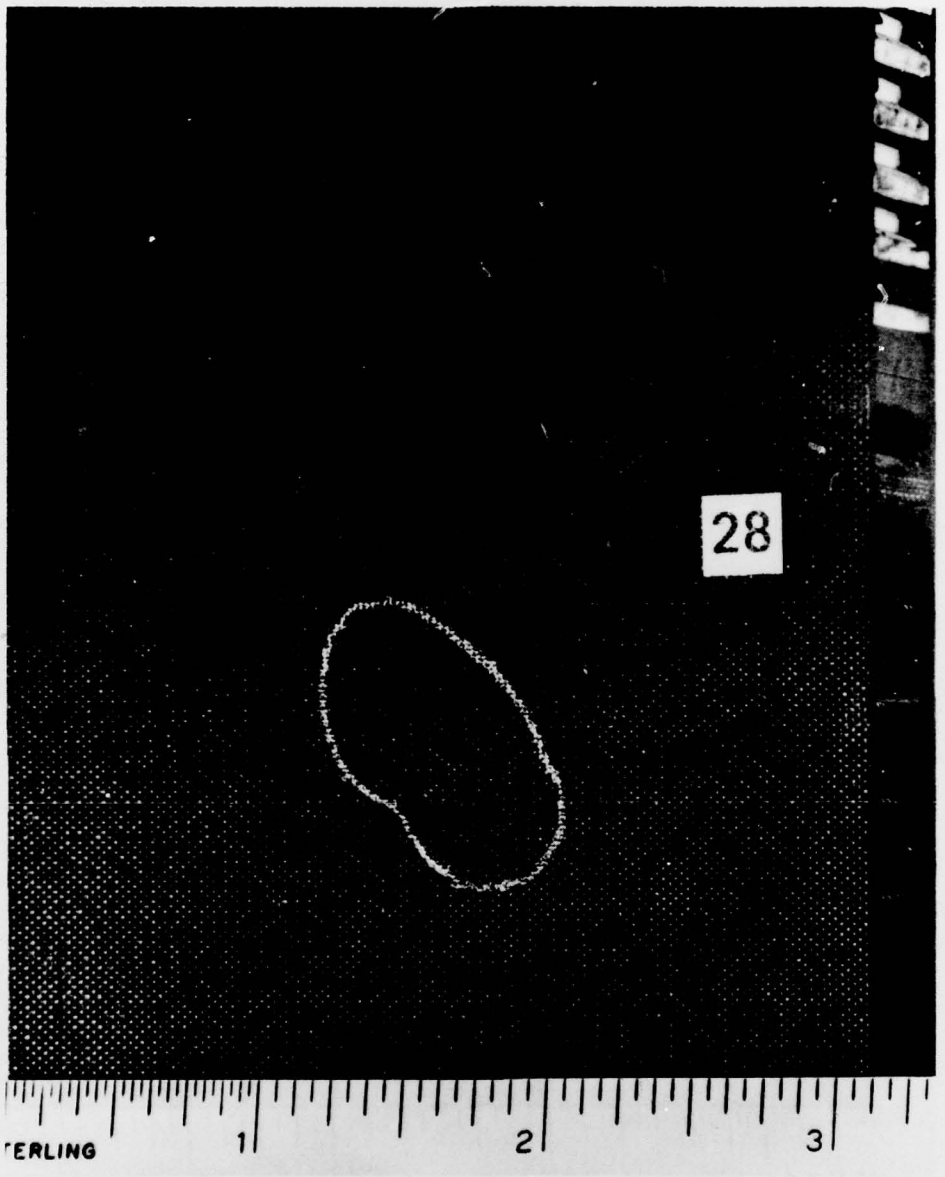

Figure 21. Damage Face for 1 inch (25.4 mm) Radius Indenter Impact of 0.500 lbm (226.8 g) at 20 ft/sec (6.1 m/s). (Delamination Outlined by White Pencil Circle)

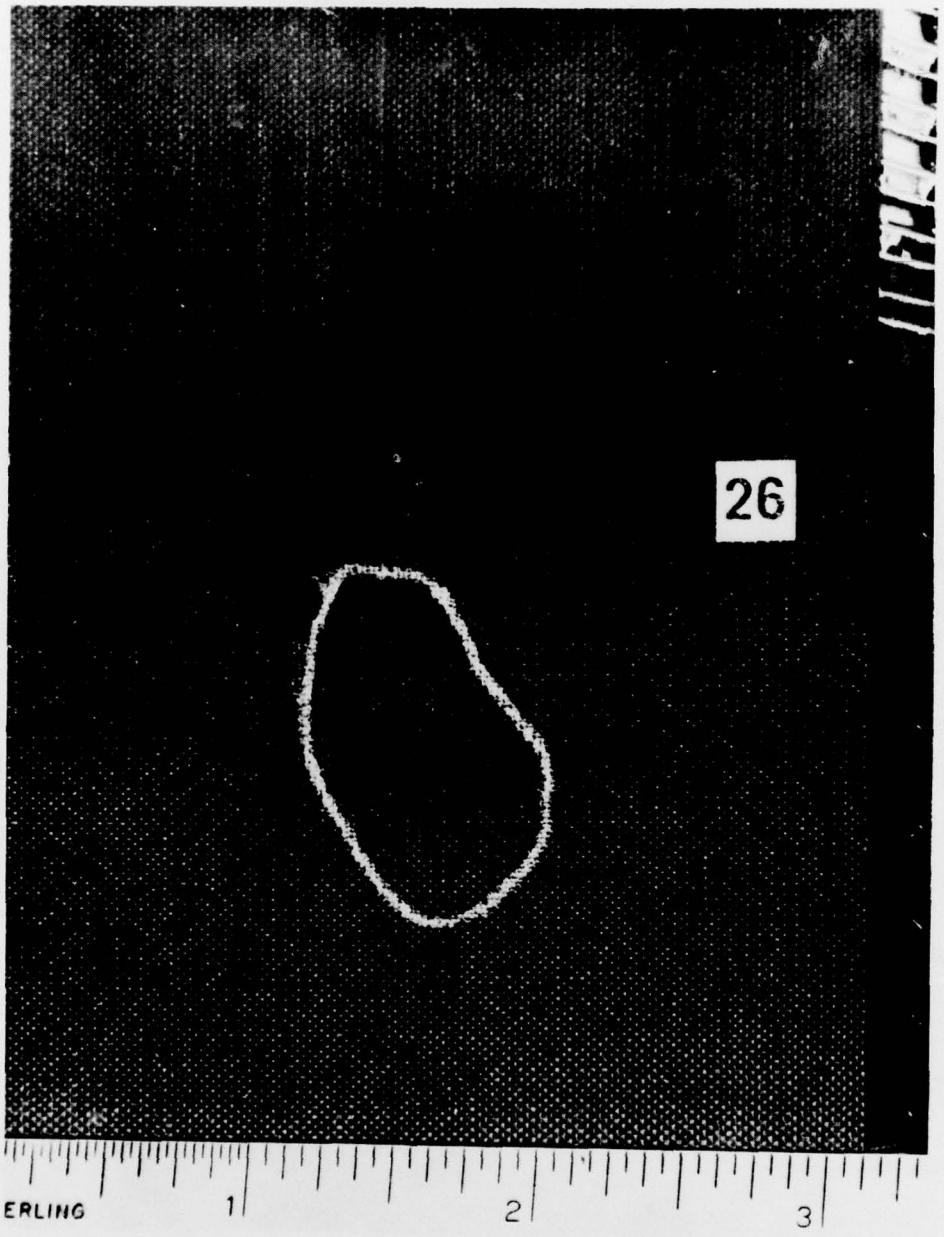

Figure 22. Damage Face for 1 inch (25.4 mm) Radius Indenter Impact of 0.800 lbm (362.9 g) at 20 ft/sec (6.1 m/s).

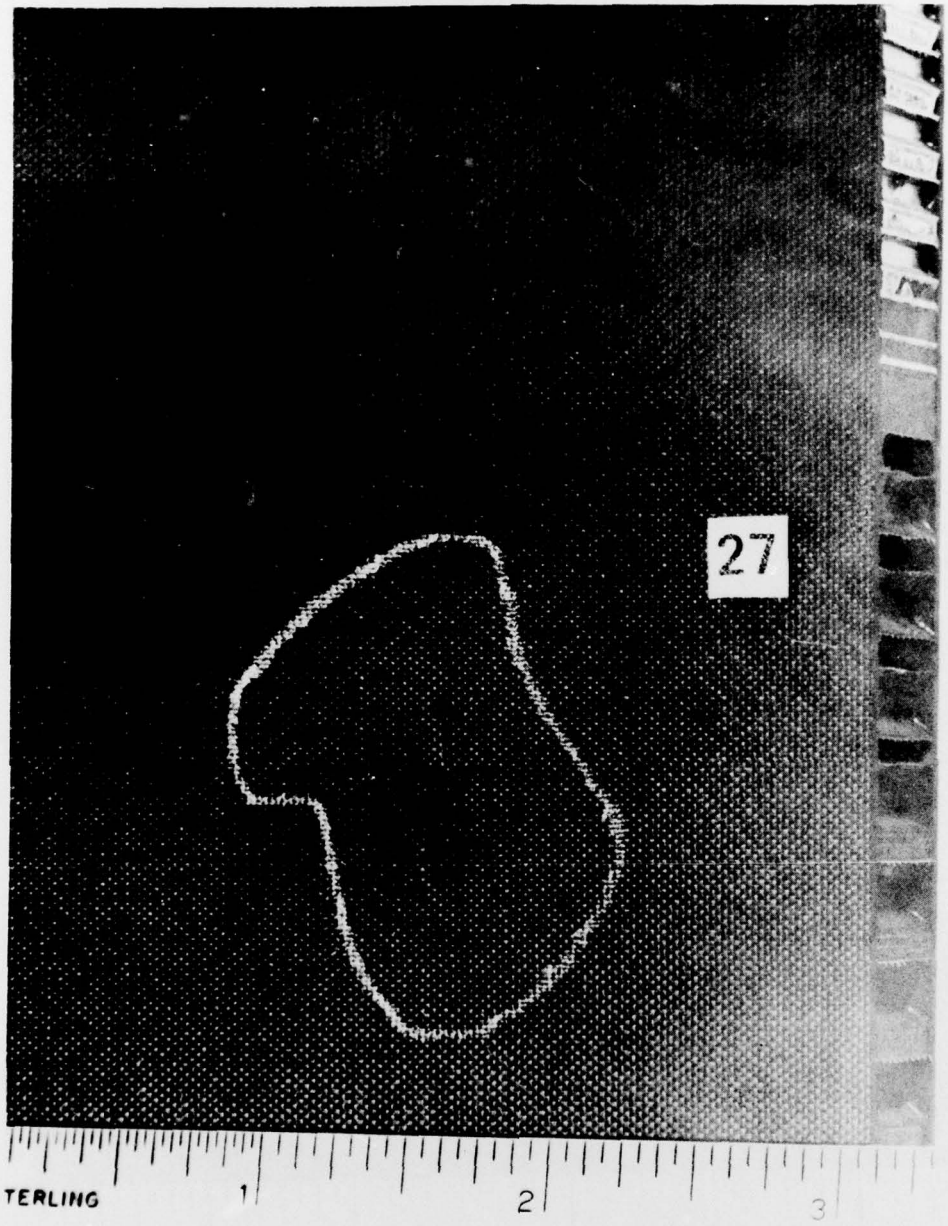

Figure 23. Damage Face for 1 inch (25.4 mm) Radius Indenter Impact of 1.50 lbm (680.4 g) at 20 ft/sec (6.1 m/s).

IMPACT TEST RESULTS

PREDICTED DAMAGE VS. MEASURED DAMAGE

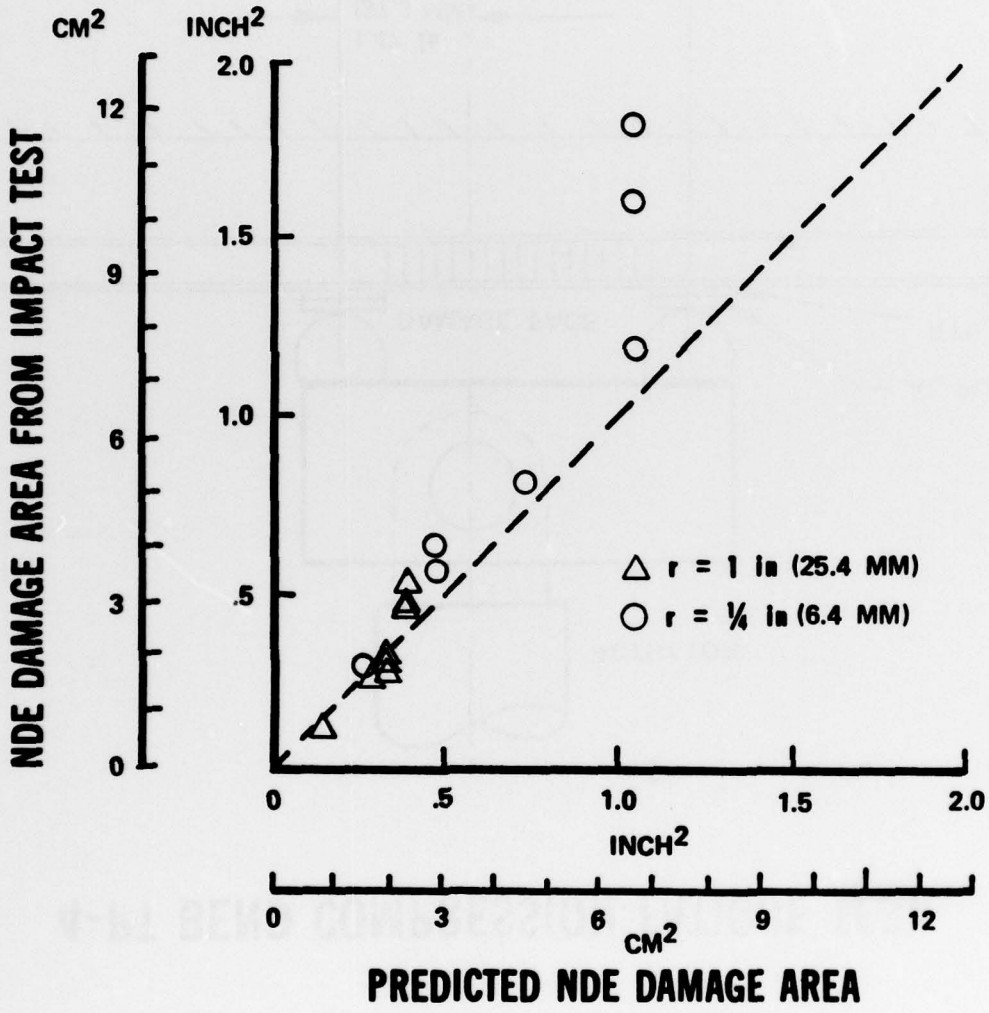

Figure 24. Predicted Impact Damage Versus Actual Damage.

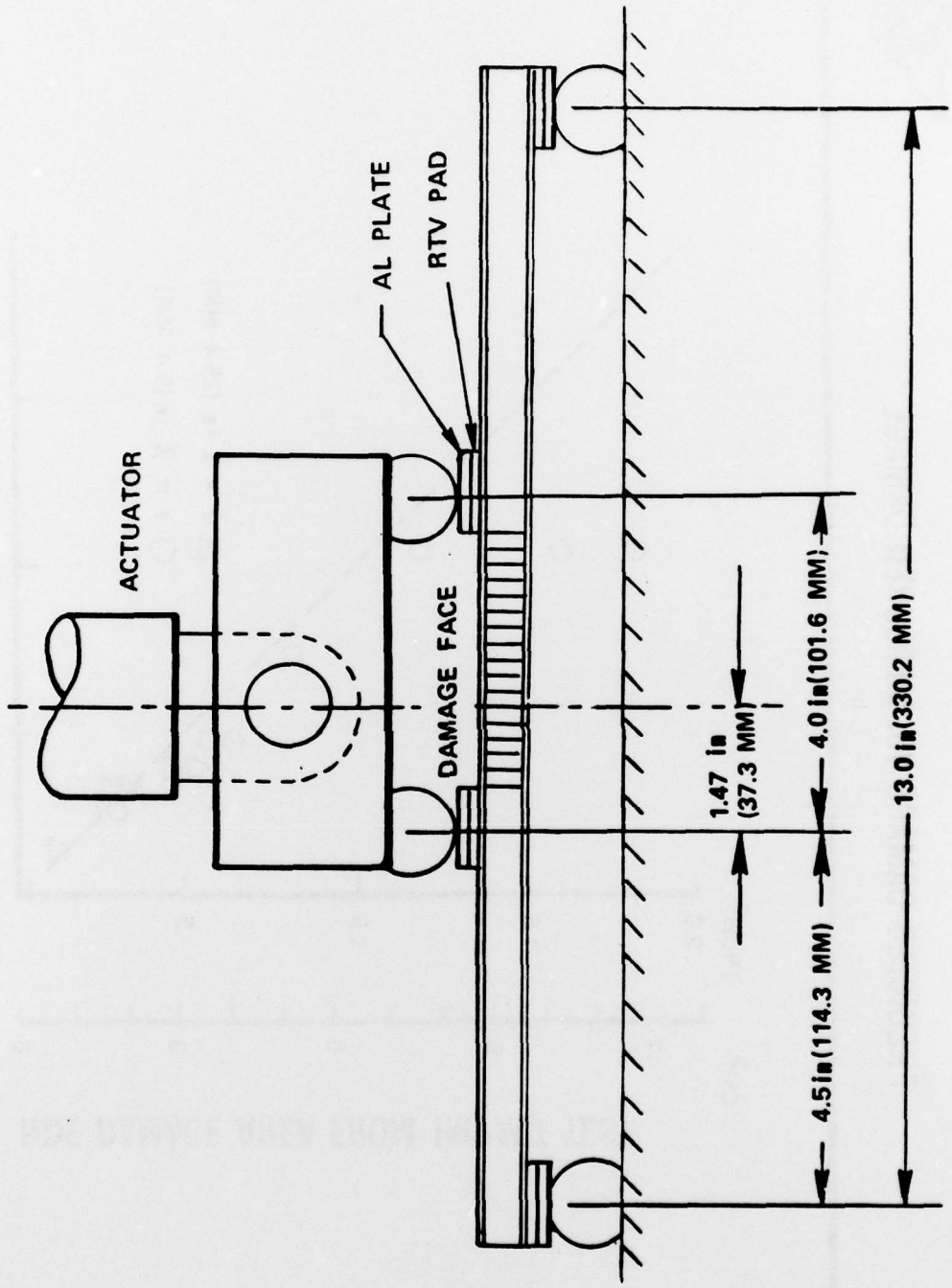

Figure 25. Fatigue Test Fixture.

Figure 26. Typical Fatigue Failure Mode

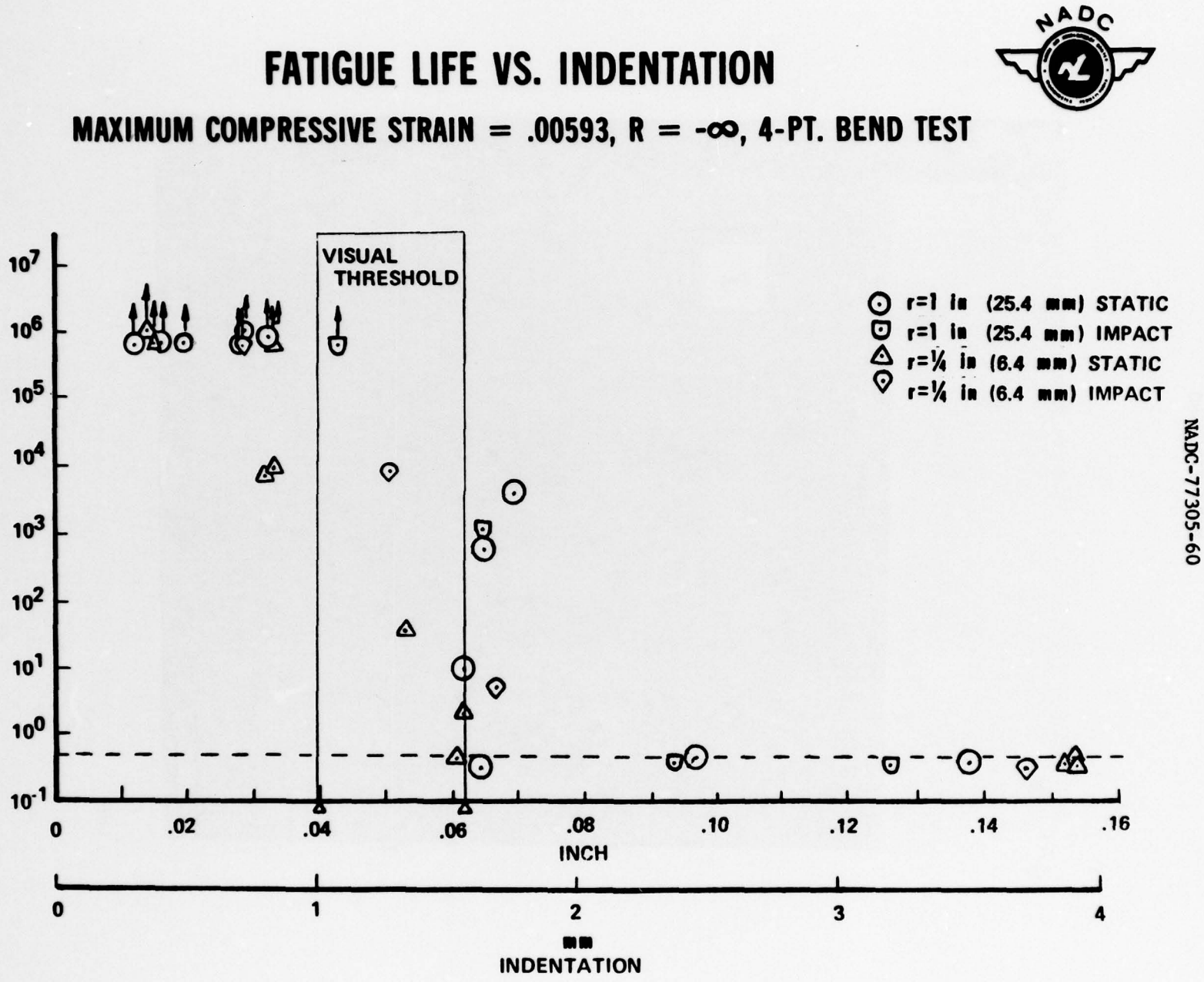

Figure 27. Cycles to Failure Versus Indentation

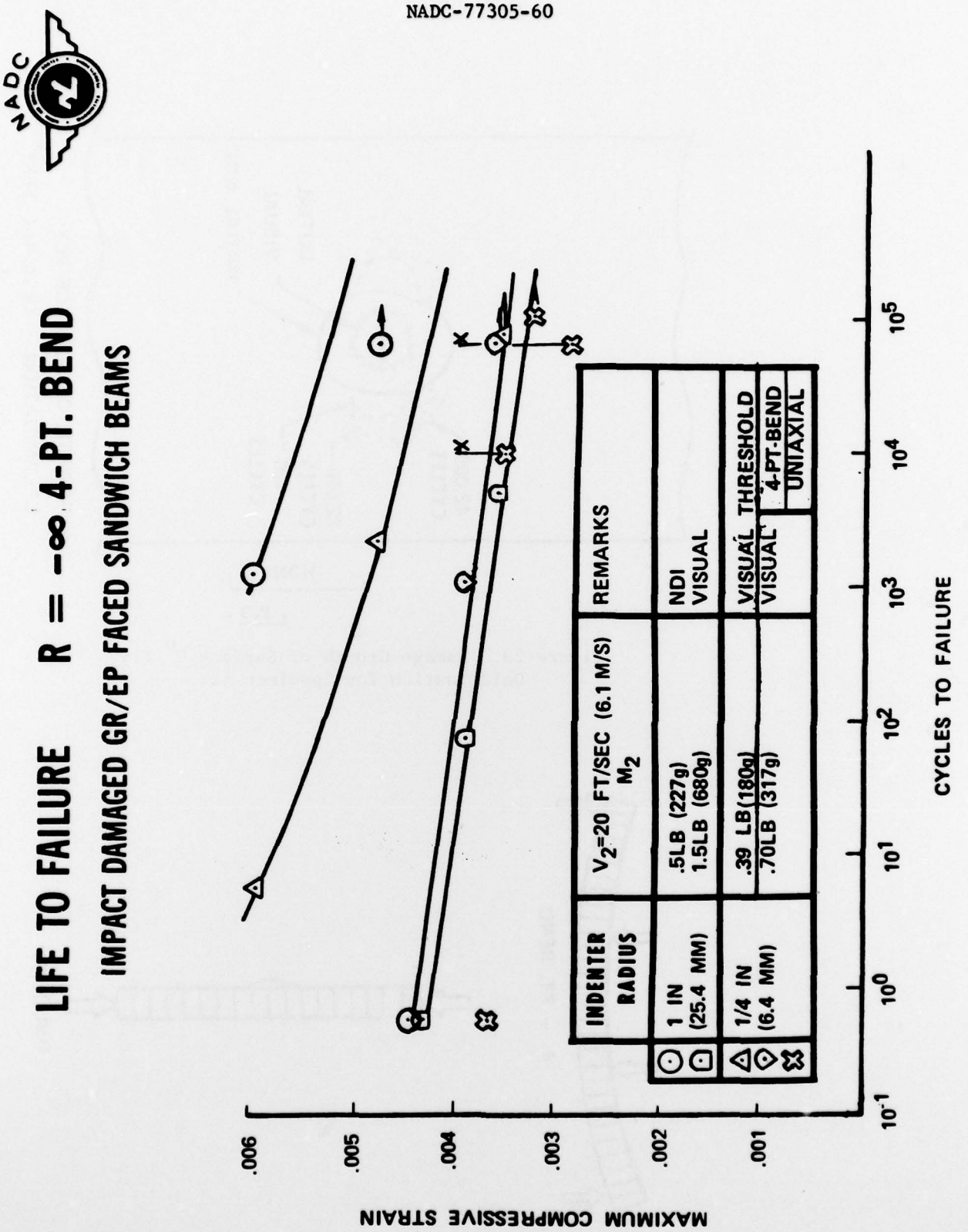

Figure 28. Life to Failure of Impact Damage Beams for R = -∞

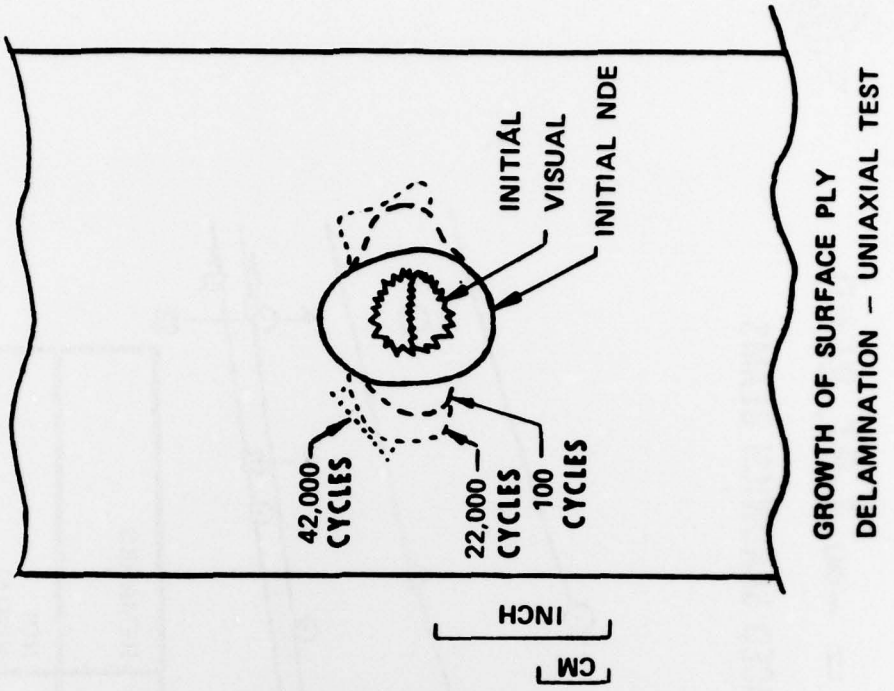

Figure 29. Damage Growth of Surface 0° Ply Delamination for Specimen 42

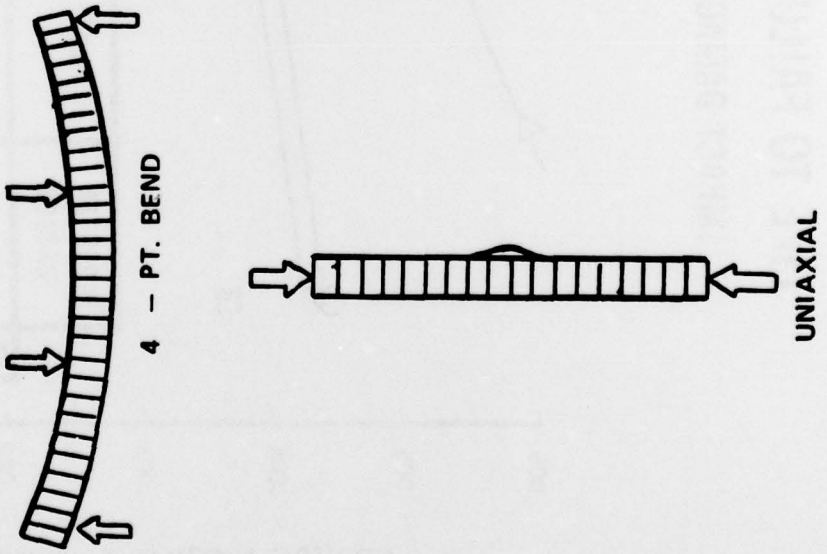

Figure 30. Four-Point-Bend Test Versus Uniaxial Compression

☆ U.S. GOVERNMENT PRINTING OFFICE: 1978-0-703-170/1015

Non-Government Agencies (Cont.)

Hercules Powder Company, Inc., Cumberland, MD 21501
(Attn: Mr. D. Hug) 1
H. I. Thompson Fiber Glass Company, Gardena, CA 90249
(Attn: Mr. N. Myers) 1
ITT Research Institute, Chicago, IL 60616
(Attn: Mr. K. Hofar) 1
J. P. Stevens & Co., Inc., N.Y., NY 10036
(Attn: Mr. H. I. Shulock). 1
Kaman Aircraft Corporation, Bloomfield, CT 06002
(Attn: Tech. Library). 1
Lehigh University, Bethlehem, PA 18015
(Attn: Dr. G. C. Sih). 1
Lockheed-California Company, Burbank, CA 91520
(Attn: Mr. E. K. Walker, R. L. Vaughn) 2
Lockheed-Georgia Company, Marietta, GA
(Attn: Advanced Composites Information Center, Dept. 72-14, Zone 42). 1
LTV Aerospace Corporation, Dallas, TX 75222
(Attn: Mr. O. E. Dhonau/2-53442, C. R. Foreman). 2
Martin Company, Baltimore, MD 21203
(Attn: Mr. J. E. Pawken) 1
Materials Sciences Corp., Blue Bell, PA 19422 1
McDonnell Douglas Corporation, St. Louis, MO 63166
(Attn: Mr. R. C. Goran, O. B. McBee, C. Stenberg). 3
McDonnell Douglas Corporation, Long Beach, CA 90801
(Attn: H. C. Schjulderup, G. Lehman) 2
Minnesota Mining and Manufacturing Company, St. Paul, MN 55104
(Attn: Mr. W. Davis) 1
Northrop Aircraft Corp., Norair Div., Hawthorne, CA 90250
(Attn: Mr. R. D. Hayes, J. V. Noyes, R. C. Isemann). 3
Rockwell International, Columbus, OH 43216
(Attn: Mr. O. G. Acker, K. Clayton). 2
Rockwell International, Los Angeles, CA 90053
(Attn: Dr. L. Lackman) 1
Rockwell International, Tulsa, OK 74151
(Attn: Mr. E. Sanders, Mr. J. H. Powell) 2
Owens Corning Fiberglass, Granville, OH 43023
(Attn: Mr. D. Mettes). 1
Rohr Corporation, Riverside, CA 92503
(Attn: Dr. F. Riel and Mr. R. Elkin) 2
Ryan Aeronautical Company, San Diego, CA 92112
(Attn: Mr. R. Long). 1
Sikorsky Aircraft, Stratford, CT 06497
(Attn: Mr. J. Ray) 1
University of Oklahoma, Norman, OK 93069
(Attn: Dr. G. M. Nordby) 1
Union Carbide Corporation, Cleveland, OH 44101
(Attn: Dr. H. F. Volk) 1

Government Activities (Cont.)

PLASTEC, Picatinny Arsenal, Dover, NJ 07801
(Attn: Librarian, Bldg. 176, SARPA-FR-M-D and Mr. H. Pebly). . 2
Scientific & Technical Information Facility, College Park, MD
(Attn: NASA Representative). 1
USAAVMATLAB, Fort Eustis, VA 23603
(Attn: Mr. R. Beresford) 1
USAMATRESAG, Watertown, MA
(Attn: Dr. E. Lenoe) 1
USARESOFC, Durham, NC 27701 1

Non-Government Agencies

Avco Aero Structures Division, Nashville, TN 37202
(Attn: Mr. W. Ottenville). 1
Battelle Columbus Laboratories, Metals and Ceramics Information
Center, 505 King Avenue, OH 43201. 1
Bell Aerospace Company, Buffalo, NY 14240
(Attn: Zone I-85, Mr. F. M. Anthony) 1
Bell Helicopter Company, Fort Worth, TX 76100
(Attn: Mr. Charles Harvey) 1
Bendix Products Aerospace Division, South Bend, IN 46619
(Attn: Mr. R. V. Cervelli) 1
Boeing Aerospace Company, P.O. Box 3999, Seattle, WA 98124
(Attn: Code 206, Mr. R. E. Horton) 1
Boeing Company, Renton, Washington 98055
(Attn: Dr. R. June). 1
Boeing Company, Vertol Division, Phila., PA 19142
(Attn: Mr. R. L. Pinckney, Mr. D. Hoffstedt) 2
Boeing Company, Wichita, KS 67210
(Attn: Mr. V. Reneau/MS 16-39) 1
Cabot Corporation, Billerica Research Center, Billerica, MA
01821 1
Drexel University, Phila., PA 19104
(Attn: Dr. P. C. Chou) 1
E.I. DuPont Company, Wilmington, DE 19898
(Attn: Dr. Carl Zweben) Bldg. 262/Room 316 1
Fairchild Industries, Hagerstown, MD 21740
(Attn: Mr. D. Ruck). 1
Georgia Institute of Technology, Atlanta, GA
(Attn: Prof. W. H. Horton) 1
General Dynamics/Convair, San Diego, CA 92138
(Attn: Mr. D. R. Dunbar, W. G. Scheck) 2
General Dynamics, Fort Worth, TX 76101
(Attn: Mr. P. D. Shockey, Dept. 23, Mail Zone P-46). 1
General Electric Company, Phila., PA 19101
(Attn: Mr. L. McCreight) 1
Great Lakes Carbon Corp., N.Y., NY 10017
(Attn: Mr. W. R. Benn, Mgr., Markey Development) 1
Grumman Aerospace Corporation, Bethpage, L.I., NY 11714
(Attn: Mr. R. Hadcock, Mr. S. Dastin). 2

DISTRIBUTION LIST

Government Activities

	No. of Copies
NAVAIRSYSCOM, AIR-954 (2 for retention), 2 for AIR-530, 1 for AIR-320B, AIR-52032D, AIR-5302, AIR-53021, AIR-530215).	9
AFFDL, WPAFB, OH 45433	
(Attn: FB/Mr. P. A. Parmley)	2
(Attn: FBC/Mr. C. Wallace)	1
(Attn: FBC/Mr. E. E. Zink)	1
AFML, WPAFB, OH 45433	
(Attn: LAM (Technical Library))	1
(Attn: LT-1/Mr. W. R. Johnston)	1
(Attn: LTF/Mr. T. Cordell)	1
(Attn: FBSC/Mr. L. Kelly)	1
(Attn: MAC/Mr. G. P. Peterson)	1
(Attn: MXA/Mr. F. J. Fechek)	1
(Attn: MBC/Mr. T. G. Reinhard, Jr.)	1
AFOSR, Washington, D.C. 20333	
(Attn: Mr. J. Pomerantz)	1
DDC	12
FAA, Airframes Branch, FS-120, Washington, D.C. 20553	
(Attn: Mr. J. Dougherty)	1
NASA (ADM), Washington, D.C. 20546	
(Attn: Secretary)	1
NASA, George C. Marshall Space Flight Center, Huntsville, AL 35812	
(Attn: S&E-ASTN-ES/Mr. E. E. Engler)	1
(Attn: S&E-ASTN-M/Mr. R. Schwinghamer)	1
(Attn: S&E-ASTM-MNM/Dr. J. M. Stuckey)	1
NASA, Langley Research Center, Hampton, VA 23365	
(Attn: Mr. J. P. Peterson, Mr. R. Pride, and Dr. M. Card)	3
NASA, Lewis Research Center, Cleveland, OH 44153	
(Attn: Technical Library, and M. Hershberg)	2
NAVPGSCHL, Monterey, CA 95940	
(Attn: Prof. R. Ball, Prof. M. H. Bank)	2
NAVSEASYSCOM, Washington, D.C. 20362	
(Attn: Code 035, Mr. C. Pohler)	1
NAVSEC, Hyattsville, MD 20782	
(Attn: Code 6101E03, Mr. W. Graner)	1
NAVSHIPRANDCEN, Bethesda, MD 20034	
(Attn: Code 173.2, Mr. W. P. Cauch)	1
NAVSHIPRANDCEN, Annapolis, MD 21402	
(Attn: Code 2870, Mr. H. Edelstein)	1
NOL, White Oak, MD 20910	
(Attn: Mr. F. R. Barnet)	1
NRL, Washington, D.C. 20375	
(Attn: Dr. I. Wolock)	1
ONR, Washington, D.C. 20362	
(Attn: Dr. N. Perrone)	1